REVIEW

Check for updates

Metal–organic frameworks and derivatives as next-generation materials for electrochemical energy storage

Xuejie Wang,[a] Zhuang Du,[b] Haiwei Tang,[a] Weilai Yu [ID] *[c] and Tao Liu [ID] *[a]

The global pursuit of carbon neutrality demands transformative clean energy solutions, with advanced energy storage materials at the forefront. Metal–organic frameworks (MOFs), owing to their tunable porosity, ultrahigh surface areas, and adaptable physicochemical properties, have rapidly risen as promising building blocks for next-generation electrochemical energy storage. Beyond pristine MOFs, engineered composites and derivatives now showcase remarkable multifunctionality, enabling improved performance in diverse battery systems. Despite this progress, significant barriers remain in translating laboratory success into practical deployment. This review provides a systematic overview of recent advances in MOF-based materials, highlighting their evolving roles as electrodes and separators in Li/Na/K-ion, Li/Na/K–S, and Zn-ion batteries. We classify design strategies by battery type, critically assess electrochemical performance, and dissect the structure–property–function relationships that underpin device operation. Finally, we outline the central challenges—stability, scalability, and interface engineering—while offering forward-looking perspectives on how to bridge these gaps. By integrating state-of-the-art progress with future opportunities, this review seeks to inspire innovative material design and accelerate the realization of sustainable MOF-based energy storage technologies.

Wider impact

The accelerating global transition toward carbon neutrality hinges on breakthroughs in sustainable, high-performance energy storage systems. Metal–organic frameworks (MOFs) and their derivatives have emerged as a uniquely versatile class of materials, offering tunable porosity, diverse chemistries, and structural adaptability that can be leveraged across a spectrum of rechargeable battery technologies. Yet, despite rapid advances, the field remains fragmented, with insights often siloed by battery chemistry or material subclass. This review bridges those divides, providing a unified, mechanism-driven analysis of MOF-based materials for Li/Na/K-ion, Li/Na/K–S, and Zn-ion batteries. By mapping structure–property–performance relationships and identifying cross-cutting challenges—such as conductivity bottlenecks, framework stability, and scalable synthesis—it offers a strategic blueprint for translating laboratory successes into commercially viable solutions. The work is intended not only for materials scientists and electrochemists, but also for engineers, policy makers, and industry stakeholders seeking to accelerate the deployment of next-generation storage technologies. By integrating fundamental understanding with forward-looking design principles, this review aims to catalyze interdisciplinary collaboration and guide the rational development of MOF-based systems that can underpin a resilient, low-carbon energy future.

1. Introduction

The depletion of fossil fuel reserves and escalating greenhouse gas emissions have precipitated a global energy crisis,

[a] Laboratory of Solar Fuel, Faculty of Materials Science and Chemistry, China University of Geosciences, 68 Jincheng Street, Wuhan 430078, P. R. China. E-mail: liutao54@cug.edu.cn

[b] Jiangsu Province Engineering Laboratory of High Efficient Energy Storage Technology and Equipments, School of Materials Science and Physics, China University of Mining and Technology, Xuzhou, Jiangsu 221116, P. R. China

[c] Department of Chemical Engineering & Applied Chemistry, University of Toronto, Toronto ON, M5S3E5, Canada. E-mail: weilai.yu@utoronto.ca

profoundly affecting socioeconomic development.[1–3] In alignment with low-carbon economy mandates and carbon neutrality objectives, the exploration of renewable and clean energy alternatives has become imperative. Nevertheless, the inherent intermittency of sustainable energy sources—such as solar and wind power—poses significant challenges to their direct large-scale utilization. Consequently, the advancement of efficient energy storage and conversion technologies has emerged as a critical research priority.[4] Rechargeable batteries have demonstrated considerable potential in grid-scale energy storage applications (Fig. 1). However, enhancing both the gravimetric and volumetric energy densities of lithium-, sodium-, potassium-,
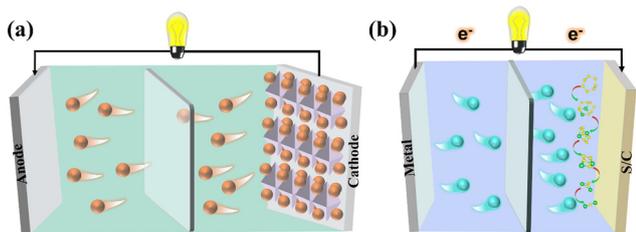
Fig. 1 The work mechanism of (a) ion-battery and (b) metal–sulfur battery.

and zinc-ion batteries (LIBs, SIBs, PIBs, ZIBs), as well as metal–sulfur systems (LSBs, SSBs, PSBs), remains essential to meet the escalating demands of next-generation energy storage solutions.

Metal–organic frameworks (MOFs) have emerged as a significant research topic in battery technology due to their superior performance compared to traditional materials.[5–7] MOFs are crystalline materials characterized by a periodic network structure formed by the self-assembly of various metal nodes and polydentate organic ligands connected by strong ligand bonds. Since Yaghi and colleagues first defined this class of materials,[8] they have attracted significant attention over the past two decades, with more than 20 000 types reported.[9,10] MOFs possess excellent properties, including a rich pore structure, structural diversity, high surface area, and multifunctionality, leading to wide-ranging applications.[11,12] Furthermore, MOF composites and derivatives developed from original MOFs have expanded their possible applications.[13]

Improving the electrical conductivity of pristine MOF materials is essential for advancing their applications in electrochemical energy storage. In recent decades, researchers have focused on developing new conductive MOF materials by modifying organic ligands. These efforts have led to remarkable electrochemical performance in supercapacitors and other energy storage devices.[14,15] In addition, the conductivity of pristine MOF materials can be significantly enhanced through the incorporation of highly conductive polymers (such as polypyrrole[16,17] and polyaniline[18,19]) and conductive carbon materials (including carbon nanotubes,[20] graphene[21,22] and carbon fibers[23]). During the pyrolysis process at elevated temperatures, the organic ligands present in the pristine MOF can transform into forms with excellent electrical conductivity. The resulting MOF derivatives have garnered considerable attention in the energy storage sector in recent years. High-temperature pyrolysis techniques can also synthesize metal compounds, metal clusters, and carbon materials in single-atom and multimetal alloys. This process typically allows for the preservation of non-metallic elements, such as nitrogen and oxygen, from the organic ligands. Following high-temperature thermal polymerization, these elements contribute to the formation of heteroatom-doped carbon, enhancing the electrical conductivity of the carbon materials and creating reactive active sites.[24–26] Composites made from MOF derivatives combine the exceptional properties of these materials with other substances, resulting in a synergistic effect where the combined performance exceeds the sum of their capabilities. This characteristic has garnered significant interest, particularly in energy storage and conversion. The advancement of MOF derivative complexes, which exhibit high catalytic activity and excellent electrochemical performance, optimally utilizes the strengths of both components, significantly enhancing the performance of rechargeable batteries.

MOFs have emerged as one of the most versatile material platforms for next-generation rechargeable batteries, owing to their tunable porosity, structural diversity, and rich functionalization potential. Recent progress has demonstrated that MOF-based materials can significantly enhance battery performance, yet realizing their full potential requires more than incremental advances—it demands rational design strategies that align material properties with the unique requirements of each energy storage technology. Although there are currently many reviews on the application of MOF-based materials in the field of electrochemical energy storage, these reviews are mainly based on the inductive summary of MOF materials and their derivatives for electrochemical energy storage,[5,15,27,28] lacking a systematic summary of the structure–property-function of MOF-based materials for electrochemical energy storage. Pang et al. reviewed recent advances in metal–organic framework (MOF)-based composites for electrochemical energy storage. While they provided detailed discussions of various MOF-based composite materials, they did not analyze the relationships between the structures and performance of these composites, nor the pros and cons of using such materials.[5] Although Zhang et al. provided a comprehensive review of the extensive applications of MOF-based materials in electrochemical energy storage, recent developments still require further detailed summarization and discussion.[27] In this review, we present a systematic overview of recent developments in MOF-based materials for rechargeable batteries, spanning lithium-, sodium-, and potassium-ion batteries, as well as lithium-, sodium-, and potassium–sulfur systems and zinc-ion batteries (Fig. 2). We analyze the principles governing MOF utilization in these systems from both material selection and structural engineering perspectives, emphasizing the critical factors that dictate electrochemical performance. Finally, we discuss the persistent challenges that hinder practical applications and outline emerging strategies to overcome them. By integrating these insights, this review aims to provide a roadmap for advancing MOF-based materials toward high-performance, sustainable energy storage devices.

2. Classification of MOFs-based materials

2.1. Pristine MOF

MOFs are crystalline materials characterized by a porous structure and a three-dimensional topological arrangement, arising from the self-assembly of metal nodes and organic ligands. The coordination dynamics of the ligands and metal nodes—including the angles formed during coordination and the lengths of
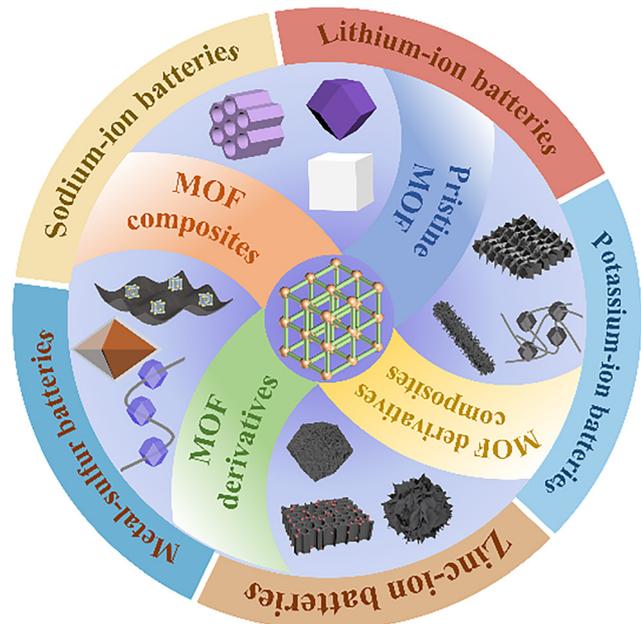
Fig. 2 Schematic illustration of the original MOF, MOF composites, MOF derivative, and MOF derivative composites.

the bonds—significantly influence the pore structure and properties of the resulting MOFs. The diversity in the choice of metal nodes and organic ligands imparts unique compositional and structural advantages to MOFs, resulting in a wide array of physical and chemical properties.[29,30] However, the insulating characteristics of the organic ligands, coupled with the unfavorable overlap between the p and d-orbitals of metal ions, typically lead to poor electrical conductivity in pristine MOF materials (often less than 10^{-10} S cm^{-1}). This presents a notable drawback for their application in electrochemical energy conversion.[31,32] Nonetheless, the abundant pore structure, high specific surface area, and stable architecture of MOFs offer ample reaction space, allowing for enhanced exposure of active sites. As a result, they demonstrate high catalytic efficiency in various catalytic processes.

Recent years have seen continuous advancements in the development of conductive MOFs to address the issue of their poor conductivity. By modifying the ligands and coordination structures, researchers have been able to enhance the conductivity of these materials to levels of 10^{-2} S cm^{-1} and higher. The integration of conductive MOFs with high specific surface areas and conductive properties has opened new avenues in the field of electrochemistry. Since the first conductive MOF was reported in 2009,[33] there has been a surge of interest in materials research,[34] culminating in the remarkable achievement of a conductivity level of 1580 S cm^{-1} reported in 2015,[35] which meets the demands of various electrochemical applications. Key factors in enhancing the conductivity of MOFs include improving carrier concentration and mobility. For MOF materials, high-energy electrons in metal nodes or redox-active ligands serve to increase carrier concentration. On the other hand, enhancing carrier mobility can be achieved through optimizing the spatial and energetic overlap of orbitals within the MOF, as improved orbital overlap effectively boosts the carrier mobility of the framework.

The primary challenge confronting MOF-based materials in electrochemical energy storage applications is the balance between structural stability and electrical conductivity. During cycling, factors such as erosion from organic electrolytes, stresses from repeated ion insertion and extraction, and electrochemical instability at operating potentials can easily lead to the collapse or deactivation of their porous crystalline structures. In recent years, research efforts have transitioned from a singular focus on achieving high specific surface areas to the development of more robust frameworks.[12,17,18,20,23,31] For instance, employing a conductive polypyrrole framework as a connecting "chain" to connect the Mg-MOF cavities effectively enhances the electrochemical kinetics and presents an impressive stability. More advanced strategies involve compositing these materials with graphene or carbon nanotubes to form three-dimensional conductive networks, or directly using them as precursors for pyrolysis to prepare metal compound/porous carbon composites.[5,19,21] All the approaches inherit the morphology and porosity advantages of MOFs while achieving outstanding chemical stability and conductivity. It has become a research hotspot for high-performance battery hosts or anode materials, demonstrating a shift in solution strategy from "passive defense" to "active conversion".

To date, various forms of MOFs have been extensively studied and utilized in the field of electrochemical energy storage, demonstrating exceptional electrochemical performance. However, pristine MOF materials present several challenges, including lower conductivity, reduced initial coulombic efficiency due to their high specific surface area, limited corrosion resistance, and lower weight density because of their greater mass. These limitations hinder their large-scale application in electrochemical energy storage. Post-processing techniques for pristine MOF materials offer potential solutions to these issues. Strategies such as functional group modification, the incorporation of active molecules, and the creation of composite multi-metal nodes can effectively enhance the components and structure of pristine MOFs, thereby broadening their application prospects in energy storage and conversion.

2.2. The combination of MOF with functional materials

The functionality of a single pristine MOF material faces numerous limitations when subjected to the high demands of electrochemical energy storage devices. Combining pristine MOF materials with auxiliary materials is an effective strategy to expand their application in energy storage.[36–38] Common auxiliary materials, such as carbon nanotubes, graphene, conductive polymers, organic molecular ligands, and metal ions, are introduced to mitigate the disadvantages of the pristine MOF materials, enhance the reactive sites, and improve conductivity.[39] In various application scenarios, selecting appropriate auxiliary materials can significantly leverage the inherent advantages of MOF materials. In the realm of electrochemical energy storage, enhancing electrical conductivity is

often the primary challenge. A prevalent approach to address this issue is the incorporation of higher conductivity carbon materials. For instance, the *in situ* growth of the pristine MOF material on carbon nanotubes can create a tandem structure, facilitating the formation of conductive channels in a one-dimensional direction.[40,41] Similarly, growing the pristine MOF on the surface of graphene not only establishes a two-dimensional conductive network but also helps prevent the stacking of MOF particles with graphene layers.[42,43] Additionally, coating the MOF particles with conductive polymers can generate a three-dimensional conductive network throughout the electrode, significantly improving the electrical conductivity of the pristine MOF material and thereby enhancing its electrochemical performance.

However, when composing the pristine MOF material with other auxiliary materials, it is important to consider the consistent uniformity of growth. Reasonable control of the ratio of the pristine MOF material to the auxiliary materials is key to preparing high-performance MOF composites. As auxiliary materials, they mainly play a role in adjusting the physicochemical properties of the pristine MOF material itself, accelerating the rate of electron transfer and improving the rate of electrochemical reaction, *etc.* In addition, while enhancing the properties of the MOF material, it is also necessary to consider whether the introduced auxiliary materials will have an impact on the advantages of MOF itself, such as leading to the clogging of the pore structure of the MOF, which affects the penetration of the electrolyte and the transport of ions; the process of preparation of the MOF material has any influence on the structural stability of the MOF material, which ultimately leads to unsatisfactory electrochemical performance.

2.3. MOF-derived carbon-based materials and their composites with functional substrate

The organic ligands in MOFs can be converted into carbon composites with outstanding electrical conductivity through post-processing in a high-temperature protective atmosphere. This transformation is rapidly emerging as an ideal approach for developing carbon materials in electrochemical energy storage.[44] A significant challenge in utilizing pristine MOF materials and their complexes in electrochemistry is their poor electrical conductivity. However, high-temperature carbonization treatments provide a practical pathway for utilizing MOF-based materials to enhance electrochemical energy storage. Furthermore, the stability of MOF materials against electrolyte degradation and their long cycle life under a broad range of voltage operating conditions have somewhat restricted their application potential. By considering the coordination modes, compositional components, and structural characteristics of the MOFs, the organic ligands can be converted into hetero-atom-doped carbon under high-temperature protective conditions. The metal ions within these frameworks can further facilitate the graphitization of the carbon material during high-temperature processing, thereby improving its electrical conductivity.[13,45] Additionally, the periodic coordination structure of the original MOF can preserve its inherent porous

nature throughout the post-treatment, resulting in carbon materials characterized by a porous structure with numerous active sites. However, to achieve the desired outcomes when preparing MOF derivatives at elevated temperatures, it is essential to carefully control processing conditions, including temperature, heating rate, protective atmosphere, and treatment duration. Based on these design principles, various composite carbon materials can be synthesized, such as metal oxide, nitride, sulfide, and selenide composites, as well as single- or dual-atom metal composites and non-metallic multi-atom doped carbon materials.[46] The variety of post-processing methods available allows for a wide range of applications for MOF derivatives, showcasing significant potential in the fields of energy storage and conversion.

Although MOF-derived carbon materials effectively address the inherent limitations related to the electrical conductivity of the original MOFs, single metal compound carbon composites continue to encounter challenges. These limitations include a scarcity of active sites, the discontinuity of individual MOF-derived particles, and issues of particle stacking. Additionally, the anisotropic nature of pyrolysis leads to shrinkage and collapse, adversely affecting the pore structure and specific surface area of the MOF derivatives, thereby constraining the applicability of MOF-derived materials. In recent years, extensive research on MOF-derived composites has demonstrated significant enhancements in performance within the domain of electrochemical energy storage.[47] MOF-derived composites can be categorized into various dimensional constructs (Fig. 3), including zero-dimensional nanoparticle composites,[48,49] one-dimensional nanofiber or nanotube composites,[50,51] two-dimensional layered nanosheet composites,[52,53] and three-dimensional architectures.

Zero-dimensional nanoparticles typically adhere to the surfaces of MOF-derived materials, or heterometallic atoms are incorporated during the synthesis of the pristine MOFs. These MOF derivatives are subsequently formed through high-temperature calcination or hydrothermal/solvent-thermal methods.
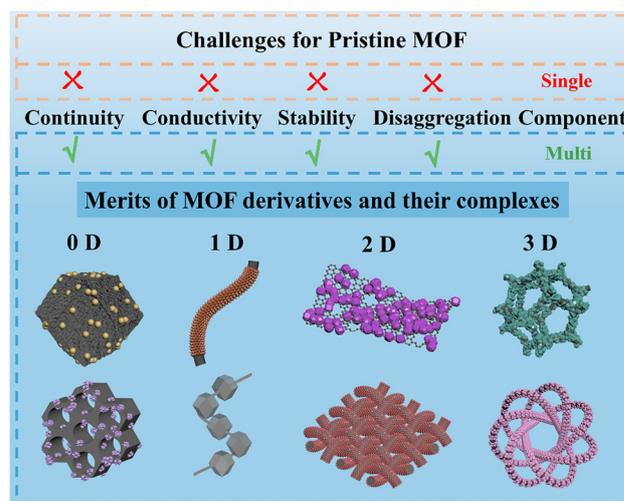

Fig. 3 Merits and classification of MOF derivative complexes.

The complexes generated through this approach not only exhibit a rich array of electrochemically active sites but also possess heterostructures that confer superior electrochemical properties when compared to single-component systems.

The one-dimensional composite methodology primarily involves the growth of original MOFs on substrates such as carbon fibers or carbon nanotubes, followed by the preparation of MOF-derived complexes *via* high-temperature pyrolysis or ion etching/exchange. Moreover, by utilizing polymer or melt solutions containing the original MOF materials, composites may be generated through a combination of electrostatic spinning technology alongside pyrolysis or similar techniques. This one-dimensional material composite strategy effectively mitigates the discontinuity of MOF-derived particles, thereby enhancing the electron transport rate along a one-dimensional axis, bolstering the high-rate performance of energy storage devices.

Two-dimensional composites frequently incorporate materials such as graphene or MXenes, known for their minimal thickness and high carrier mobility. Through *in situ* growth, electrostatic interactions, and post-processing techniques, MOF-derived composites are prepared. This approach yields a two-dimensional framework that facilitates rapid charge transport and minimizes the aggregation of MOF particles and two-dimensional materials, thus significantly enhancing the material's potential for energy storage applications.

Three-dimensional MOF composites are engineered through techniques such as *in situ* growth coating, spray drying, and *in situ* polymerization. Following these processes, further treatment methods, including pyrolysis and hydrothermal/solvent-thermal processing, are applied to yield interactive three-dimensional structures. These methodologies not only foster the formation of three-dimensional electron transport networks but also prevent particle accumulation, preserving the structural integrity of the MOF materials. As a result, the developed three-dimensional MOF-derived composites exhibit remarkable advantages in the realms of electrochemical energy storage and conversion.

Despite substantial progress in MOF-derived composites, the field remains largely exploratory: key interfacial phenomena that ultimately determine device lifetimes and kinetics are still poorly controlled and poorly understood. Critical unknowns include how heteroatom distributions, residual metal species, and anisotropic shrinkage during pyrolysis set the local chemistry and porosity at carbon–metal/oxide interfaces; how these interfacial motifs govern charge-carrier pathways, ion transport, and the nucleation/evolution of interphases (*e.g.*, SEI/CEI or polysulfide adsorption layers); and how mesoscale architecture (pore connectivity, tortuosity, and heterostructure contacts) couples to atomistic reaction pathways. Closing these gaps will require coordinated studies that link synthetic "knobs"—ligand chemistry, node composition, templating, defect engineering, and thermal profiles—to measurable interfacial signatures using *operando*, high-resolution probes (cryo-TEM, *operando* XPS/IR, ToF-SIMS, synchrotron scattering) together with multiscale modelling (DFT → MD → continuum models). Establishing standardized model systems and quantitative interfacial metrics will accelerate the derivation of transferable design rules, enabling MOF-derived composites to move from promising demonstrations to robust, high-efficiency energy-storage components.

3. The applications of MOFs and their derivatives for Li/Na/K-ions batteries

The rapid development of LIBs over recent decades has led to widespread use in electric vehicles and various portable electronic devices.[54,55] However, the energy density of Li-ion batteries is nearing its limits, making it difficult to meet the growing requirements of advanced electronic devices. Additionally, the depletion of raw materials and rising costs associated with extensive lithium resource consumption hinder the progression of the new energy industry. Fortunately, sodium and potassium—elements in the same main group—are abundant and function similarly to lithium in LIB applications, positioning them as promising candidates for the next generation of rechargeable batteries. Nevertheless, the high standard potentials of sodium (−2.71 V) and potassium (−2.93 V), compared to lithium (−3.045 V), along with their larger ionic radius, result in considerable volume expansion during cycling, which presents challenges for the development of Na/K-ion batteries. Consequently, innovation in novel and high-efficiency electrode materials has become a focal point of research aimed at overcoming these limitations. Metal-ion batteries consist of an anode, cathode, separator, and electrolyte, with each component playing a critical role in determining the overall performance. Research and development innovation in these materials is essential for enhancing the energy density of metal-ion batteries. MOFs, composed of organic ligands and metal ion clusters, provide abundant pore space for ion storage and feature highly active metal sites that serve as attractive locations for electrochemical reactions. This unique structure endows MOFs with significant advantages in the application of metal-ion batteries.

3.1. Pristine MOF

Thanks to their high specific surface area, abundant pore structures, and active sites, MOFs have garnered considerable attention in recent decades for their application in metal-ion batteries. However, their low electrical conductivity and poor stability during cycling pose significant challenges that limit their practical use. Current research efforts focus on enhancing the stability of electrochemical reactions, creating multiple reaction sites, and improving conductivity to achieve superior performance.

The 2D Fe-MOF (Fe-TABQ), featuring reversible metal and ligand redox processes, comprises square planar Fe–N_2O_2 bonds and phenylenediamine building blocks, resulting in a π–d-conjugated structure within the 2D plane. Fe-TABQ demonstrates remarkable capacity retention in lithium storage, attributed to its double-ionic reactive active sites, along with the inherently robust Fe–N (O) bonds and enhanced Li–N (O) bonds
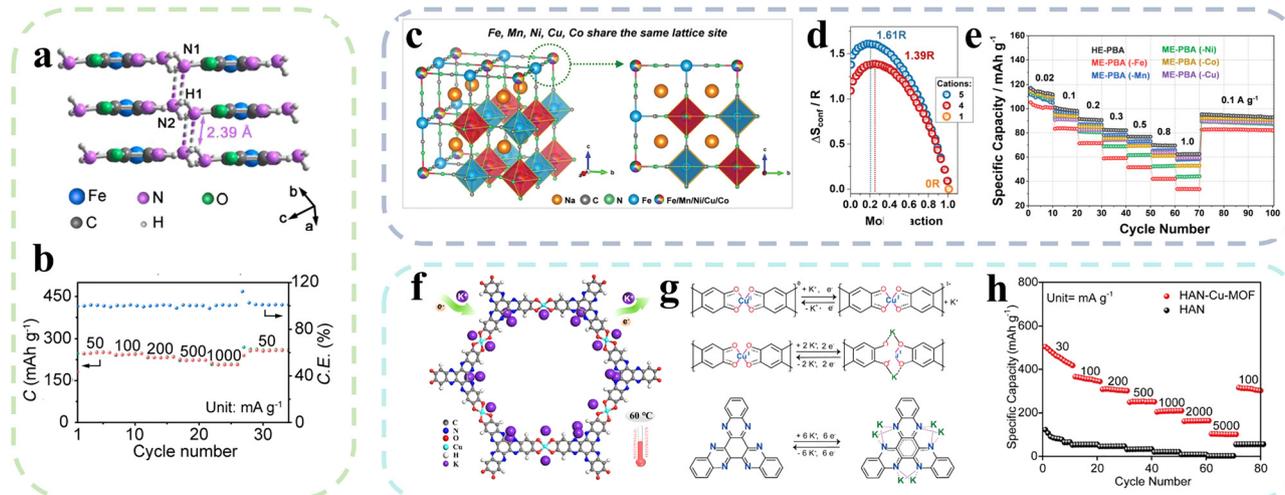
Fig. 4 Pristine MOF materials for LIB, SIBs, and PIBs. (a) Structural illustration of Fe-TABQ and (b) the rate performance.[56] Copyright © 2023, American Chemical Society. (c) The crystal structure of HE-PBA, (d) The dependence of configurational entropy on the number of elements and (e) the rate performance.[57] Copyright © 2021, Wiley–VCH. (f and g) Schematic of the K⁺ storage process in HAN-Cu-MOF, CuO₄ and HAN units; (h) rate performance.[58] Copyright © 2024, American Chemical Society.

(Fig. 4a and b).[56] Novel CoBPDCA MOF materials, formed from cobalt(II) nitrate and 2,2-bipyridyl-4,4-dicarboxylic acid (BPDCA), exhibit dual active sites from both Co ions and BPDCA ligands (–C=N and –C=O). With excellent electrochemical stability and high conductivity, the resulting hexagonal CoBPDCA achieves an impressive reversible capacity of 1112.9 mAh g⁻¹ at 0.05C (1C = 1000 mAh g⁻¹), alongside outstanding high-rate durability, maintaining 166.3 mAh g⁻¹ after 2500 cycles at 10C.[59] The development of functionalized multi-thiol-supported dicarboxylate-based metal–organic framework (Fe-TTTP) highlights the dual reactive active sites of iron(III) ions and organic dicarboxylate ligands, which display excellent electrochemical properties. Thanks to its unique chemical structure and insolubility, Fe-TTTP significantly enhances both rate and capacity performance in dicarboxylate-based MOF materials. It achieves a remarkable rate performance of 950 mAh g⁻¹ at 50 mA g⁻¹ and maintains 95 mAh g⁻¹ even at a high current of 10 A g⁻¹, along with a prolonged cycle life of 310 mAh g⁻¹ over 5000 cycles at 2 A g⁻¹.[60]

In the field of SIBs, pristine MOFs primarily employed for sodium storage consist of Prussian blue (PB) and its analogs (PBA). These materials exhibit three-dimensional open frameworks that provide substantial sodium storage capacity, thereby facilitating the rapid insertion and extraction of sodium ions during the charging and discharging processes.[61] Ma et al. developed a high-efficiency PBA (HE-PBA) using a co-deposition method at room temperature, wherein five metals were integrated into identical nitrogen ligand sites (Fig. 4c–e). This methodology resulted in an entropy increase exceeding 1.5 R for the entire system. Notably, the HE-PBA demonstrated a zero-strain mechanism during the electrochemical sodium storage process, showcasing remarkable cycling stability and rate performance, achieving over 3000 cycles and a coulombic efficiency approaching 100%.[57] In addition to PB and PBA,

other MOF materials with distinctive structural characteristics are also being investigated as electrode materials for SIBs. For example, Bao et al. synthesized a cobalt-based hexaiminobenzene (Co-HAB) MOF featuring a d–π conjugated extended two-dimensional conductive structure tailored for sodium ion storage. This material benefits from both a high specific surface area and a two-dimensional conductive framework, which promote enhanced diffusion and charge transport kinetics of sodium ions, resulting in high reversible capacity and exceptional cycling stability.[62]

Potassium ions exhibit a limited cycling lifetime due to their larger ionic radius, which hinders diffusion within the crystal structure and leads to structural collapse caused by significant volume expansion. Chen et al.[63] constructed an amide-functionalized 2D Cu-HBB-MOF with multiple active sites for potassium-ion battery anode materials through an in situ metal coordination-induced planarization strategy. It exhibited excellent potassium storage capacity and cycling stability, providing insights into the design of multiple active site 2D MOFs, salicylamide framework coordination modification, and metal active center exploration. The vanadium-based MOF material, MIL-47, features dual active sites and extensive layer spacing. In this framework, the reversible rearrangement of the conjugated carboxyl group in organic terephthalic acid to an enolate form, coupled with the redox activity of vanadium ions, serves as a stable mechanism for potassium storage. Furthermore, the multichannel structure, facilitated by the bridging of vanadium to the unsaturated functional groups within MIL-47, enhances the transport of both ions and electrons.[64] As a result, this material demonstrates excellent electrochemical performance when employed as electrodes in potassium ion batteries. High-temperature potassium ion batteries represent a significant trend in this field; however, the interface between the electrode and electrolyte at elevated temperatures can initiate severe side

reactions. This may lead to the degradation of the phase structure within the solid electrolyte interface and a loss of electrochemical reversibility. Therefore, it is essential to ensure the stability of potassium-ion battery (KIB) anodes under high-temperature conditions. In response to this challenge, Li *et al.* developed a porous conducting MOF utilizing nitrogen-rich aromatic molecules and CuO_4 units through π–d conjugation. This MOF provides a wealth of active sites and demonstrates exceptional structural stability (Fig. 4f–h).[58] The dual redox active sites of the C=N groups and CuO_4 units, along with the reticulated porous structure enabled by the π–d conjugation, facilitate the rapid transport of K^+/e^- while maintaining minimal volume expansion of the insoluble electrode. Consequently, this results in a stable high-capacity potassium storage capability, achieving 96.7% capacity retention over 1600 cycles.

While pristine MOFs have garnered significant attention and research within the realm of metal-ion batteries, their inherent limitations continue to restrict their practical application. Although pristine MOFs offer a rich pore structure and numerous active sites in comparison to commercial electrode materials, challenges such as higher costs, low conductivity, reduced initial coulombic efficiency, irreversible phase transitions, and inadequate resistance to electrolyte corrosion still hinder their direct use as electrode materials for metal-ion batteries.

3.2. Composite MOF and functional materials

The development of MOF composites is an effective strategy to address their limitations. By retaining the original MOF to enhance pore structure and active sites, the introduction of supplemental materials can improve drawbacks such as structural stability and electrical conductivity of the original MOF materials. Carbon materials, renowned for their excellent electrical conductivity—such as CNTs and graphene—are frequently utilized in the preparation of MOF composites. These carbon materials, with their spatial electronic conductivity, can enhance both the structural stability and electron transport rate of the original MOF materials. For instance, the *in situ* growth of Al-MOF ($Al(OH)[O_2C–C_6H_4–CO_2]$) particles on graphene, achieved through the dual modulation of electrostatic attraction and non-homogeneous nucleation, significantly improves electrical conductivity and structural stability (Fig. 5a).[65] This composite demonstrates exceptional electrochemical performance when employed as an anode in LIBs, maintaining a specific capacity of 282.0 mAh g^{-1} even after 2000 cycles at 2 A g^{-1}, indicating an ultra-long cycle life and excellent lithium storage capability. In another study, Qiao *et al.* prepared $Ni(BDC-NH_2)$/reduced graphene oxide (rGO) composites *via* a hydrothermal method, subsequently fabricating freestanding and lightweight composite electrodes for lithium-ion battery anodes through vacuum filtration.[66] The designed structures feature rGO nanosheets tightly enveloping $Ni(BDC-NH_2)$ flakes, resulting in synergistic enhancements. The rGO serves to spatially separate the particles, preventing aggregation of MOF particles and effectively increasing the electrode–electrolyte contact interface. Additionally, the three-dimensional interaction structure established by rGO helps mitigate volume expansion of the MOF material during lithium storage, while also fostering rapid electron and ion transport through a conductive network. The small particle size of $Ni(BDC-NH_2)$ reduces the transport distance for Li^+/electron, thereby accelerating the reaction kinetics. The composite electrodes for LIBs exhibit remarkable discharge-specific capacity and rate performance.

In addition to incorporating carbon materials into the original MOF composite, combining MOF materials with organic
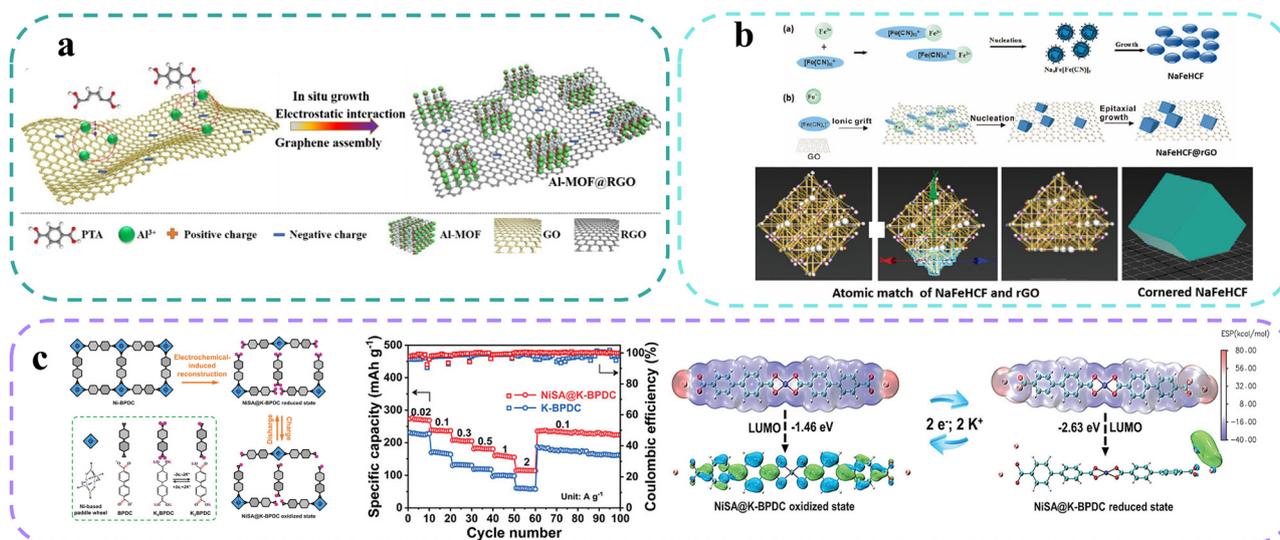

Fig. 5 The applications of MOF composites for LIB, SIBs, and PIBs. (a) Schematic illustration of the preparation processes of Al-MOF@RGO composites and the electronic conductivity and transport ability of Li^+ ions.[65] Copyright © 2023, Elsevier. (b) Structural diagrams of cubic and cornered NaFeHCF and TEM images.[70] Copyright © 2024, Wiley–VCH. (c) Schematic illustration to prepare NiSA@K-BPDC and the chemical structure, ESP images, and LUMO energy levels of NiSA@K-BPDC anodes during cycling.[71] Copyright © 2024, Wiley–VCH.

compounds is also an attractive strategy.[7,67] Li et al. constructed a three-dimensional structural film by growing ZIF-8 nanoscale units on polyimide nanofibers, which was used as a separator for lithium metal batteries.[38] While ensuring efficient ion transport, the material offers advantages like thermal stability, mechanical flexibility, and high safety, demonstrating highly beneficial electrochemical performance when used as a separator for lithium metal batteries. Sun et al. used In-based MOFs and poly(vinylidene fluoride–hexafluoropropylene) (PVH) to prepare solid-state polymer electrolytes for all-solid-state lithium metal batteries, achieving extremely high ionic conductivity and excellent electrochemical performance.[12] MOF-based materials have great application potential in the field of electrochemical energy storage for the composite construction of high-performance separators or multifunctional layers.

Prussian blue analogues (PBAs) demonstrate a robust three-dimensional architecture characterized by open ion diffusion channels and numerous electrochemically active sites, thereby exhibiting remarkable electrochemical performance as cathode materials in SIBs.[3,68] In a notable study conducted by Cui et al., Nickel-based Prussian blue (Ni-PBA) was in situ synthesized into an inverted pyramid structure within sodium citrate-derived three-dimensional ultrathin porous carbon (3DUC), facilitating enhanced ion and charge transport.[69] The inverted pyramid configuration exhibits a strong adhesion to 3DUS throughout the growth process, resulting in a stable structural framework. This methodology effectively mitigates the tendencies for particle aggregation and rapid nucleation associated with Ni-PBA. Consequently, the interaction structure significantly reduces the ion diffusion distance and lowers the diffusion barrier for Na^+, thereby augmenting sodium storage capacity. However, the structural regularity of PBAs is frequently compromised due to a high prevalence of $[Fe(CN)_6]$ defects and an uncontrollable crystallization rate during synthesis. Such disruptions lead to structural collapse during Na^+ insertion and extraction processes, which in turn hinders the migration of ions and electrons within the framework, increases electrode polarization voltage, and ultimately undermines the multiplicative performance of the cell. In response to these challenges, Jiang et al. adopted an epitaxial nucleation growth strategy to enhance the lattice regularity of PBAs (Fig. 5b).[70] By utilizing GO as a substrate, they capitalized on the perfect lattice matching between sodium iron hexacyanoferrate (NaFeHCF) and GO. The electronegative functional groups present on the GO surface (–COOH, –OH, –CH(O)CH–) serve as nucleation sites, thus guiding the subsequent crystallization of NaFeHCF. This approach effectively improves the lattice regularity of NaFeHCF and promotes rapid ion diffusion within the structure. Furthermore, the dispersive properties of GO facilitate a reduction in particle size and enhance the uniformity of the dispersion, which collectively shortens the migration pathway for Na^+ and promotes electrolyte penetration. The highly conductive reduced graphene oxide (rGO) obtained through the reduction of GO contributes two-dimensional planar electronic conduction while simultaneously acting as a protective layer to inhibit undesired side reactions. Through the synergistic

effects of structural integrity and morphological optimization, the synthesized NaFeHCF@rGO demonstrates high reversible capacity and prolonged cycle stability.

Anode materials composed of redox-active organic compounds, such as potassium 1,1′-biphenyl-4,4′-dicarboxylate (K-BPDC), have garnered significant attention in the realm of potassium ion batteries. However, their slow reaction kinetics and instability pose challenges for practical applications in PIBs. He et al. employed an electrochemically induced reconstituting strategy to incorporate nickel single atoms into K-BPDC, thereby enhancing its reaction kinetics and stability as an electrode material for PIBs (Fig. 5c).[71] The introduction of single-atom nickel facilitated local charge rearrangement within K-BPDC, accelerated the migration rate of K^+ ions, reduced the potential barrier, and kinetically improved the reversible opening of the conjugated carbonyl (C=O) in K-BPDC. The resulting NiSA@K-BPDC anode, created using this method, demonstrates significant enhancements in capacity, reaction kinetics, and cycling performance. Conversely, the growth of dendrites and the substantial volume expansion of potassium metal anodes limit their commercial viability. To develop a dendrite-free potassium metal anode with long-cycle stability, Luo et al. designed a lightweight, flexible 3D composite host material (CNT@ZIF-8) by combining ZIF-8 with CNT.[72] The abundance of potassiophilic N/Zn active nucleation sites, a high specific surface area, and a porous structure within ZIF-8 effectively promote K^+ diffusion kinetics and facilitate uniform deposition at the anode. Due to reduced concentration gradients and uniform nucleation on the negative electrode surface, the K@CNT@ZIF-8 anode exhibits remarkable cycling stability of 3200 hours. Additionally, the fully prepared cell demonstrates improved cycling stability and rate performance.

3.3. MOF derivatives carbon-based materials

Despite the remarkable electrochemical performance of pristine MOF materials and their composites in metal-ion batteries, their limited conductivity and structural stability pose significant challenges for broader applications in this field. During thermal polymerization, the organic ligands found in MOFs can transform into graphitized carbon materials. Under high temperature and calcined atmosphere conditions, metal sources within the MOFs can be converted into metals and their compounds. Additionally, the calcination conditions allow for adjustments to the three-dimensional framework of pristine MOF materials, facilitating the preparation of carbon materials with a porous structure. These carbon materials serve dual purposes: acting as electronic conductors and providing micro/mesoporous adsorptive sites for metal ion storage. Concurrently, the metals and their compounds contribute to enhanced discharge capacity through alloying and conversion reactions. Thanks to their exceptional properties, MOF derivatives have garnered significant research interest in the realm of electrochemical energy storage in recent years.

Mao et al. synthesized ZIF-8 particles with varying particle sizes and morphologies by modulating the mass ratio of zinc salt to 2-methylimidazole.[73] This approach facilitated the

subsequent production of nitrogen-doped porous carbon with distinct dimensions *via* high-temperature calcination. The resulting material demonstrated exceptional electrochemical performance in LIB/SIBs, attributable to its diminutive size, nitrogen content, and mesoporous and microporous characteristics. Lang *et al.* employed liquid gallium-assisted pyrolysis on the metal–organic framework ZIF-67, yielding nitrogen-doped CNTs with non-hollow frameworks encapsulating cobalt (Co) nanoparticles.[74] Following acid etching, CNT structures with nitrogen and oxygen-containing functional groups were derived and utilized as anode materials for SIBs. The metal–organic framework (MOF)-derived pure carbon materials exhibited remarkable rate performance and stable long-cycle capability for sodium storage, achieving a discharge capacity of 185 mAh g^{-1} at a current density of 10 A g^{-1}, alongside ultra-stable cyclability over 20 000 cycles.

However, it is noteworthy that graphitized carbon materials typically possess low discharge capacities. Furthermore, multi-electron conversion reactions, facilitated by the presence of metal compounds in the electrochemical process, tend to exhibit theoretical capacities significantly exceeding those of traditional graphite anodes. The development of metal compound/graphitized carbon composites is a promising strategy. It merges the high electronic conductivity of graphitized carbon with the advantageous multi-electron conversion properties of metal compounds, thereby showcasing superior electrochemical performance in metal-ion batteries. Huang *et al.* prepared carbon nanoboxes embedded with dispersed Co_3O_4 hollow nanoparticles as anode materials for LIBs through a combination of chemical etching-coordination and subsequent two-step annealing processes.[77] The unique structural attributes of these nanoboxes, characterized by an abundance of active sites and substantial volumetric space, translated to excellent electrochemical performance for lithium storage. The cubic-structured

MOF-derived metal compound/porous carbon architecture retained the porous characteristics of the original MOF throughout the etching and calcination phases. This structural integrity, combined with uniformly dispersed metal compound nanoparticles within the three-dimensional framework, facilitated optimal lithium ion adsorption on the carbon material and promoted an efficient multi-electron transfer process involving the metal compound.

In a related study, Yu *et al.* synthesized hollow carbon mesoporous shells (CoS/C HC) containing nanoscale CoS nanoparticles *via* a high-temperature carbothermal reduction and sulfidation of the ZIF-67 precursor, subsequently investigating its sodium storage behavior and electrochemical performance in sodium-ion capacitors (Fig. 6a–d).[49] The presence of a multitude of electron-transfer active sites and conductive interfaces conferred exceptional and stable long-cycle capability and high-rate performance for sodium storage. The comprehensive electrochemical performance of CoS/C HC produced through this methodology surpassed that of conventional CoS carbon materials, attributable not only to the structural advantages conferred by the original MOF but also to the mesoporous architecture that significantly enhances sodium ion adsorption while mitigating volume expansion during sodium storage—key factors in achieving optimal rate capabilities and long-cycle stability.[78] Moreover, the abundant pore structure and active metal sites of pristine MOF materials serve as effective precursor substrates for electrode material fabrication. $Cu_3(BTC)_2$ (HKUST-1), a copper-based cubic MOF, showcases a unique three-dimensional porous structure characterized by large and open pore channels facilitated by its copper ion-organic ligand connectivity.[79] This distinctive morphology allows for comprehensive contact with reactants, leading to the formation of small and uniform target product particles. Tang *et al.* processed HKUST-1 through high-energy ball milling and high-temperature
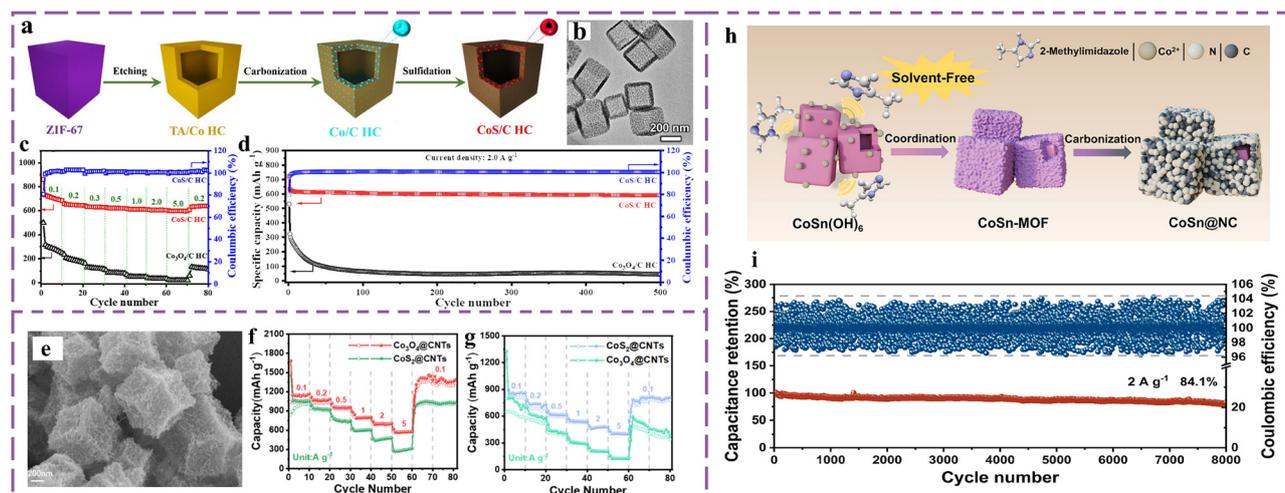
Fig. 6 The applications of MOF derivatives for LIBs, SIBs, and PIBs. (a) Synthetic process, (b) TEM image, (c) rate and (d) cycle performance of CoS/C HC.[49] Copyright © 2023, Elsevier. (e) SEM image of Co@CNTs; the rate performances of Co_3O_4@CNTs and CoS_2@CNTs for (f) LIB and (g) SIB.[75] Copyright © 2024, American Chemical Society. (h) Schematic illustration for synthetic carbon-coated CoSn alloy (CoSn@NC) and (i) the cycle performance of Li-ion capacitors.[76] Copyright © 2024, Elsevier.

calcination, in conjunction with TiO_2 and Li_2CO_3 using a solid-phase reaction method, to produce ultra-small $Li_2CuTi_3O_8$@H-KUST particles. The carbon links existing between these particles, along with the external carbon layer, provided an excellent conduction pathway, thus enhancing electronic conductivity under conditions of high magnification.[80] As an anode material for LIBs, this approach resulted in elevated lithium ion diffusion rates, high reversible capacities, and extended cycle stability compared to systems utilizing copper salts as precursors. The use of MOF materials characterized by favorable periodicity as precursors for developing high-performance electrode materials presents an effective strategy, maximizing the structural benefits and uniformly dispersed metal active sites inherent to MOFs.

The cost-effective advantages of sodium resources position them as promising candidates for next-generation rechargeable batteries. However, the development of SIBs is significantly hindered by several key constraints, including the large ionic radius associated with sodium ions, which results in low ion mobility, substantial volume changes, and sluggish kinetics. A viable strategy for enhancing the performance of SIBs involves synthesizing transition metal compounds (TMCs) with carbon materials that exhibit high-capacity properties due to multielectronic reactions. Central to this endeavor is the identification and optimization of active sites within metal compounds, particularly those involved in conversion reactions. In this context, the use of Zeolitic Imidazolate Framework-67 (ZIF-67) as a precursor facilitates the preparation of MOF-Derived Co_3O_4@CNT and CoS_2@CNT anodes through high-temperature calcination and vulcanization techniques (Fig. 6e–g).[75] This composite strategy, which integrates N-doped carbon nanotube (CNT) conductive frameworks with metal compounds, effectively addresses the bulk effects associated with TMCs, thereby enhancing the overall conductivity of the electrodes. In comparative analyses, Co_3O_4@CNT has shown superior lithium storage performance relative to CoS_2@CNT in LIBs. Conversely, this trend is inverted in SIBs, thereby highlighting the distinct differences between lithium and sodium storage mechanisms. Metal oxides typically exhibit stable crystal structures that help maintain cycling performance over extended periods, due to the smaller ionic radius of lithium. In contrast, the more reactive metal sulfide structures, such as CoS_2, may undergo structural alterations and phase transitions during lithium-ion storage, ultimately leading to degradation in long-term cycling performance. For SIBs, the larger ionic radius of sodium induces significant volume expansion during cycling, which can damage the lattice structures of metal oxides, consequently diminishing their electrochemical performance. The structural integration of CoS_2 nanoparticles, uniformly encapsulated within dodecahedral carbon shells and supplemented by nitrogen-doped CNTs, effectively mitigates volume expansion during charge and discharge cycles while significantly enhancing material conductivity. Consequently, contemporary research into anode materials for SIBs has increasingly concentrated on highly reactive metal sulfides, selenides, and phosphides, which have demonstrated exceptional sodium storage capabilities.

The volumetric expansion and structural disruption associated with the larger ionic radius of potassium ions contribute to diminished stability and compromised electrochemical performance of the electrode materials. Consequently, investigating electrode materials capable of facilitating K^+ intercalation and deintercalation, with a focus on crystal structure, reaction mechanisms, and related characteristics, constitutes a predominant area of research within the potassium-ion battery system. MOFs and their derivatives present a promising avenue for potassium storage, given their rich pore structures. Furthermore, composite materials derived from metal active sites capable of multi-electronic transitions can significantly enhance the potassium storage performance. Graphite, known for its chemical stability and electrical conductivity, stands out as an exemplary material for metal ion storage, especially due to its advantageous electrochemical properties for potassium storage. The unique structural attributes of MOF-derived carbon materials facilitate the creation of extensive channels for potassium ion diffusion while concurrently augmenting potassium storage capacity. In a notable study by Mai et al., a one-step low-temperature pyrolysis method was utilized to synthesize nanostructured graphite complexes composed of multi-walled carbon nanotubes and graphite shells.[81] This innovative approach culminated in a highly graphitized three-dimensional conductive structural network, achieving an initial coulombic efficiency (ICE) of up to 80% and demonstrating remarkable cycling stability over 1000 cycles at 500 mA g^{-1}. Despite these advances, pure carbon materials often exhibit limited potassium storage capacity and suboptimal reaction kinetics during the potassium storage process, impeding the realization of high-capacity, high-energy density, and rapid-performance potassium storage systems.

The incorporation of heteroatoms enriches the active sites for potassium storage within carbon-based materials, while structural defects introduced by these heteroatoms further enhance electrical conductivity, thereby improving electrochemical performance. A series of MOF composites featuring core–shell structures was developed by Yu et al. using a straightforward synthesis strategy, which culminated in heteroatom-doped carbon materials through high-temperature pyrolysis and acid etching.[82] When used as anode materials for PIBs, the MOF-derived carbon composites, consisting of a high-conducting carbon core enveloped by nitrogen-doped carbon, exhibit exceptional potassium storage capacities. The distinct architecture and heteroatom doping characteristics yield increased active sites and expedited reaction kinetics.

Metal compound conversion anode materials are notable for their high theoretical specific capacities and redox properties, delivering commendable electrochemical performance in ion batteries. However, these materials often suffer from poor electrical conductivity and substantial volume changes during potassicization and depotassicization, leading to inadequate rate capability and rapid capacity degradation. Conversely, MOF-derived carbon/metallic compound materials exhibit abundant pore structures, excellent structural stability, and numerous active sites, thereby effectively mitigating the limitations associated with conventional carbon materials in

potassium-ion battery applications. Wang *et al.* employed a programmable strategy to utilize Sn-based MOFs as precursor materials, producing Sn-MOF materials with a superstructure, ultimately yielding $Sn_3(PO_4)_2$@phosphorus doped carbon ($Sn_3(PO_4)_2$@PC-48) *via* high-temperature thermal polymerization.[83] This product maintained the original superstructural morphology of the Sn-MOF, and the synergistic effects of this unique morphology alongside the inherent activity of $Sn_3(PO_4)_2$ lead to reduced particle size and diminished stress within the material. Consequently, this mitigates the risks of electrode pulverization and detachment during electrochemical reactions. This composite material demonstrated an impressive stability of 90.1% capacity retention after ultra-long cycling across 10 000 cycles at a current density of 5 A g^{-1}. Additionally, Zhang *et al.* synthesized three-dimensional porous nitrogen-doped carbon composites (3D Co_9S_8@NPC) featuring uniformly dispersed MOF-derived Co_9S_8 nanoparticles through the utilization of NaCl as a template and Polyacrylamide as a carbon source. During the coordination process with Co^{2+}, the nanoparticles are embedded into the pore structure of 2-methylimidazole, leading to the final composites produced *via* high-temperature thermopolymerization and subsequent removal of NaCl.[84] The rich pore structure and abundant active sites inherent in these materials effectively shorten the K^+ diffusion distance, thereby accelerating both K^+ insertion and extraction kinetics. Furthermore, the three-dimensional architecture functions as an electron transport network and alleviates the volumetric expansion of Co_9S_8, resulting in exceptional electrochemical performance and prolonged cycling stability during potassium storage.

In addition to pure carbon materials and metal compound/carbon composites, alloying reactions in metal-ion batteries play a significant role in the overall process. During the alloying phase, the electrode material interacts with lithium, sodium, or potassium to form a binary alloy. Before reaching the final state, the intermediate phase alloy undergoes a phase transition influenced by the structural characteristics of the material and the rate of lithiation, sodiation, or potassization. The ultimate alloying product defines the material's theoretical capacity and the alloying reaction volume. Anode materials based on the alloying mechanism exhibit a high theoretical capacity due to the ability to facilitate multi-electron transfers. However, with each alloying cycle, the exposure of newly formed electrode materials increases the reduction of the solution due to significant volume changes, adversely impacting the overall coulombic efficiency. Early battery failure, stemming from volume expansion and irreversible phase transitions of metals and their compounds during sodiation, presents a challenge in developing long-cycle-stable materials. To address the issue of volume change and the loss of active sites for lithium, sodium, or potassium storage, strategies such as nanosizing the active sites of metallic particles and encapsulating the nanoparticles have proven effective. Furthermore, in addition to traditional modification techniques like alloy nanosizing and surface coating, innovative approaches have emerged. These include the alloying of three-dimensional

conductive frameworks, the spontaneous formation of core–shell structures by alloy nanoparticles, and gradient alloying in negative electrodes. MOF-derived metal/carbon composites feature an open three-dimensional porous structure and conductive framework in which dispersed metal nanoparticles can be tightly confined within the carbon material during the *in situ* growth process. This arrangement effectively promotes the nanosizing of alloy-type anode materials and helps mitigate volume expansion.

Recent advancements in research on anode materials for lithium storage through alloying have yielded significant breakthroughs. The primary binary alloy anode materials examined include Si, Bi, Sn, Sb, and Ge. For instance, Yang *et al.* utilized MOF materials as precursors to successfully develop Bi@CF, which features Bi nanoparticles encapsulated in a thin carbon film *in situ*.[85] This combination of electrochemically active Bi nanoparticles with a conductive carbon matrix not only accelerates reaction kinetics but also effectively mitigates the volume expansion that occurs during the alloying and de-alloying processes, resulting in remarkable electrochemical performance (306 mAh g^{-1} after 900 cycles at 1.0 A g^{-1}). In addition to single-phase metal nanoparticles, an effective strategy involves the introduction of inert metal elements, such as Co, Fe, and Cu, to form stable intermetallic compounds.[86] For instance, CoSn alloy (CoSn@NC) materials are encapsulated with a nitrogen-doped carbon matrix derived from CoSn-MOF (Fig. 6h and i).[76] The encapsulation of the electrochemically inert Co, combined with the nitrogen-doped carbon matrix, facilitates the *in situ* generation of non-electrically active Co and establishes a robust carbon and nitrogen matrix around the CoSn alloy, which features a hollow interior structure. This configuration effectively alleviates significant volume expansion and maintains the structural integrity of the material during the lithiation process. Furthermore, the presence of highly conductive Co and N atoms enhances the electrochemical reaction kinetics and increases the overall conductivity of the material. As a result, these anodes exhibit excellent electrochemical performance and long-cycle stability when utilized in LIBs.

The metal alloying reaction is a critical process in sodium storage applications. Alloy anode materials utilized in SIBs predominantly encompass materials such as Sn, Sb, P, Ge, Bi, and Pb. Among these, Pb is particularly noteworthy due to its ability to form a binary alloy, $Na_{15}Pb_4$, upon interaction with sodium. This alloy exhibits a high sodium storage capacity of 485 mAh g^{-1} and a volumetric capacity of 5480 mAh cm^{-3}, accompanied by a favorable electrochemical potential for sodium storage. However, the substantial cyclic volume expansion (365%) associated with Pb—stemming from electrode pulverization and detachment from the current collector—poses significant challenges.[87,88] This expansion can lead to the development of unstable solid electrolyte interfaces (SEIs) and accelerated capacity decay. To mitigate these issues, approaches such as nanosizing and carbon encapsulation of Pb have emerged as effective strategies for enhancing electrical conductivity, reducing particle agglomeration, and minimizing

volume expansion. Zhao *et al.* synthesized $Pb_2(HBTC)_2 \cdot 5H_2O$ through the coordination of 1,3,5-benzenetricarboxylic acid (1,3,5-H_3BTC) with Pb^{2+} ions, subsequently producing carbon-encapsulated Pb nanospheres (Pb@C) *via* high-temperature calcination.[89] The resulting Pb nanospheres are uniformly integrated within a carbon matrix derived from organic ligands, which effectively prevents particle stacking and enhances inter-particle conductivity while facilitating particle downsizing. These materials exhibit rapid reaction kinetics and outstanding electrochemical properties during Na–Pb alloying processes for sodium storage. Furthermore, Bi is recognized as a potential anode material for sodium storage, characterized by a lower alloying/de-alloying potential (0.6 V) and larger lattice fringes (d(003) = 3.95 Å) that favor the de-embedding of sodium ions.[90,91] Bi also possesses a high theoretical capacity of 385 mAh g^{-1}; however, it is similarly susceptible to significant volumetric expansion (approximately 244%) during sodium storage, which results in electrode pulverization and rapid capacity degradation. In a notable study, Chen *et al.* developed Bi nanoparticles/N-doped carbon (Bi@NC) *via* one-step pyrolysis of a bismuth-containing metal–organic framework (Bi-MOF) precursor.[92] The resulting nanostructure features Bi nanoparticles uniformly encapsulated by N-doped carbon, effectively minimizing the migration distance for sodium ions. This configuration not only ensures rapid kinetic reactions but also mitigates electrode expansion. When utilized as anode materials in SIBs, these structures exhibited remarkable rate performance and exceptional cycle stability, maintaining a capacity of 326.9 mAh g^{-1} over 5000 cycles at a current rate of 2 A g^{-1}.

The utilization of potassium ions, which exhibit a larger ionic radius, presents distinct challenges in terms of volume expansion and capacity decay in alloy-type anodes. Among potential potassium storage materials, red phosphorus is noted for its remarkable potassium storage capacity, achieving up to 1154 mAh g^{-1} for K_4P_3. Nevertheless, its application is significantly hindered by two critical factors: the inherently poor electrical conductivity of red phosphorus and the substantial volume expansion (approximately 290% during alloying) associated with its alloying process.[93] To address these limitations, carbon materials emerge as suitable carriers for red phosphorus, given their excellent electrical conductivity and their ability to accommodate volumetric changes. Specifically, carbon derived from MOFs possesses advantageous characteristics, including a high specific surface area, a three-dimensional conductive framework, and numerous active sites and pore structures. These features facilitate the uniform loading of red phosphorus while enhancing overall conductivity. In a study conducted by Chen *et al.*, homogeneous Zn-MOF-74 hexagonal nano/micro rods with varying diameters were synthesized through a carefully controlled solvent method.[94] By employing high-temperature calcination, the pristine structural integrity of these materials was preserved, culminating in a maximum potassium storage capacity of 763 mAh g^{-1} at a 66 wt% red phosphorus loading. This enhancement in performance is attributed to the superior electrical conductivity and the effective mitigation of volume expansion provided by MOF-derived

carbon materials. The challenges associated with the pulverization of metal-phase anode materials, particularly in the pursuit of high potassium storage capacity, necessitate alternative approaches. Intermetallic compounds with multiple alloying phases have been identified as effective solutions to the single-phase pulverization typical of metal anodes, as they not only offer excellent electrical conductivity but also alleviate volumetric expansion. However, these intermetallic compounds face the issue of phase splitting during discharge, alongside alloying during the charging process, which contributes to electrode pulverization over extended cycling durations. In response, Tong *et al.* developed bismuth alloy materials with metastable states ($Bi_{0.85}Co_{0.15}$@C and $Bi_{0.83}Fe_{0.17}$@C) through the calcination of MOF precursors.[95] These materials were subsequently employed as anode components for potassium ion batteries. During the discharge cycle, active Bi and inactive Co were effectively compartmentalized into particles of approximately 10–20 nm, uniformly dispersed within the carbon matrix. Notably, the resulting two-phase metal particles formed from the discharge of the metastable BiCo alloy avoided conversion into intermetallic compounds during the charging process. The Co particles, previously inactive in electrochemical activity, were transformed into conductive metallic forms, serving to impede the reaggregation of Bi nanoparticles while enhancing the potassiumation and de-potassiumation kinetics of elemental bismuth during initial charge/discharge cycles. Thus, the design of metastable phase alloy materials effectively circumvents the ongoing phase transitions characteristic of intermetallic compounds during cycling, leading to significant mitigation of volumetric expansion.

3.4. MOF derivative composite with functional materials

The construction of composites derived from MOFs allows for the effective utilization of their remarkable structural and physicochemical properties. These carefully designed composites can synergistically leverage the advantages of multiple components, thereby enhancing electrochemical performance. In the realm of metal-ion batteries, the variations primarily include MOF-derived/carbon composites, MOF-derived/two-dimensional materials, multivariate MOF-derived heterogeneous composites, ion-doped MOF derivatives, and MOF-derived polymers, among others. Such diverse composites are advantageous for the research and development of next-generation storage batteries, particularly in terms of tailoring the properties related to morphology, structure, composition, and electronic structure.

Liu *et al.* synthesized a multilayer multifunctional skeleton utilizing oxidatively treated polyacrylonitrile (OPAN) and derivatives of MOFs *via* electrostatic spinning.[96] This innovative design aims to modulate the deposition characteristics of lithium metal anodes while effectively mitigating dendrite growth. By co-spinning and subsequently calcining ZIF-8/ZIF-67 with polyacrylonitrile (PAN), a three-dimensional conductive skeleton was developed, characterized by one-dimensional nanowires. This structure was then laminated with OPAN to achieve a rational regulation of lithium-ion flux, distribution of nucleation sites, and enhanced electrical conductivity.
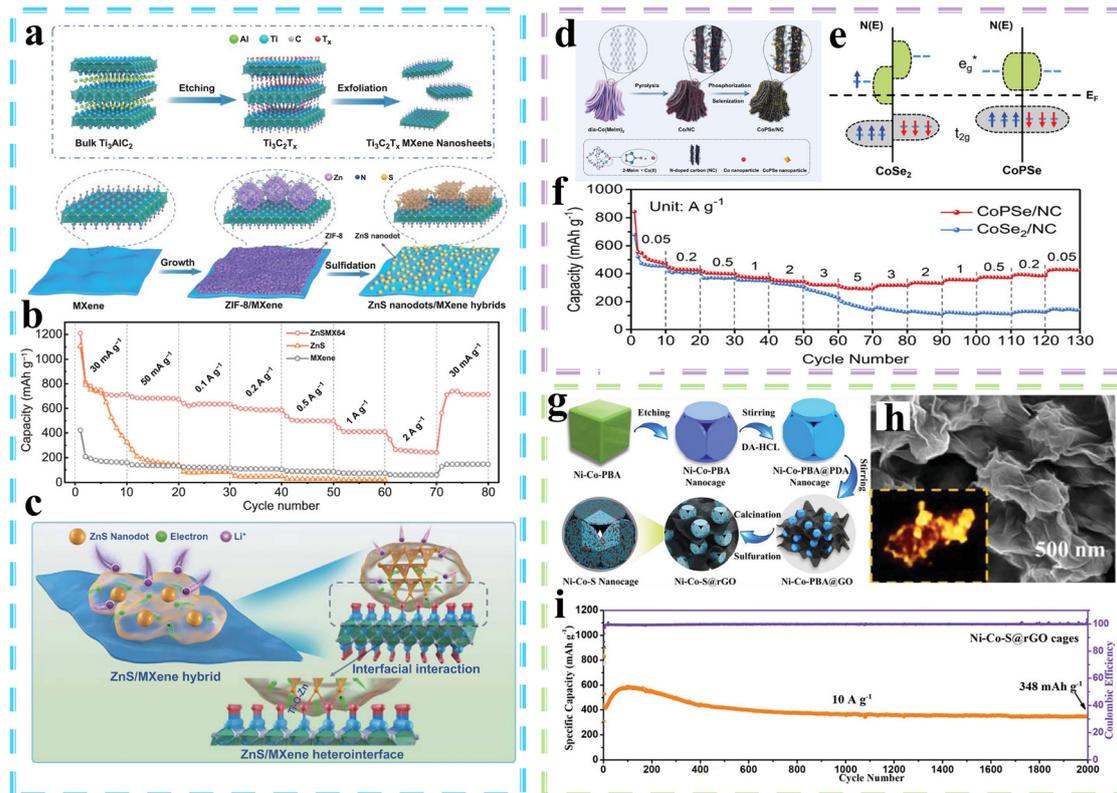
Fig. 7 The applications of MOF derivative composites for LIBs, SIBs, and PIBs. (a) Schematic illustration for the synthesis of ZnS/MXene hybrids; (b) rate performance and (c) Interfacial interaction mechanism.[97] Copyright 2021 Springer Nature. (d) The synthesis process of the CoPSe/NC composite; (e) Energy level diagrams of the frontier molecular orbitals for pyrite-phase $CoSe_2$ and CoPSe structures; (f) Rate performance.[102] Copyright © 2021, Wiley–VCH. (g) Schematic illustration of the Ni–Co–S@rGO cage nanocomposites; (h) TEM image; (i) cycle performance.[103] Copyright © 2022, Wiley–VCH.

The strong interactions of the functional groups C≡N, C=N, and C=O in OPAN with lithium ions promote uniform lithium-ion deposition within the three-dimensional framework. The one-dimensional MOF-derived structure, composed of electrostatically spun filaments, alongside its porous architecture and electron transport network, facilitates both ion adsorption and deposition at high current densities. Furthermore, the composite film, featuring alternating insulating and conducting layers, effectively suppresses the formation of lithium dendrites, showcasing unique advantages in the regulation of lithium deposition behavior. MOF derivative/two-dimensional material composites have emerged as a promising strategy to address the stacking and discontinuity challenges associated with MOF particles, thus proving advantageous for developing high-performance electrode materials. In a related investigation, Cao *et al.* engineered zero-dimensional to two-dimensional ZnS nanodots/$Ti_3C_2T_x$ complexes, which comprise ZnS nanodots modified on $Ti_3C_2T_x$ MXene nanosheets (Fig. 7a–c).[97] These ZnS nanodots facilitate a reduction in the diffusion distance of lithium ions and enhance electrochemical kinetics. Simultaneously, the $Ti_3C_2T_x$ nanosheets provide a rapid pathway for electron transport within a two-dimensional plane and inhibit the aggregation of ZnS nanoparticles, while also accommodating volumetric expansions of ZnS during charge–discharge cycles. Additionally, the robust bonding at the Ti–O–Zn interface effectively anchors the ZnS

nanoparticles to the $Ti_3C_2T_x$ nanosheets, thereby preventing detachment from the conductive substrate. This innovative 0D–2D ZnS nanodots/$Ti_3C_2T_x$ composite exhibits remarkable lithium storage capacity and cycling stability. Recent studies have widely explored various composite structures derived from MOFs, including $CoFe_2O_4$/$Ti_3C_2T_x$ MXene/carbon nanofiber, sandwich-structured complexes[98] and graphene-coated $NiCo_2O_4$–NiO–Co complexes,[53,99] highlighting the significance of interfacial coupling between MOF derivatives and two-dimensional materials in enhancing the electrochemical performance of LIBs. When two-phase materials interface, variations in the electronic structure at the contact surface arise due to disparities in Fermi energy levels, carrier types, and concentrations. This transformation bestows the heterostructured materials with superior electron transport properties, abundant active sites, and enhanced catalytic activity, making them up-and-coming candidates for applications in energy storage technologies.[100] Zhang *et al.* further advanced the field by fabricating one-dimensional core–shell structured ZnSe@CoSe@CN heterostructured materials.[101] Utilizing a high-temperature treatment strategy on dopamine-coated ZIF-8@ZIF-67 pristine MOF materials, they developed N-doped carbon-coated ZnSe/CoSe nanodots. The hollow structure of these one-dimensional materials effectively mitigates volume expansion during electrochemical reactions, maintaining the structural integrity of the anode. The high surface area and aspect ratio of the hollow morphology promote insertion

and desorption processes for metal ions, as well as efficient electrolyte infiltration. The nanoscale dimensions of ZnSe and CoSe significantly shorten the diffusion pathways for Li^+/Na^+, simultaneously alleviating mechanical stress. The non-homogeneous lattice interfaces within the structure facilitate accelerated Li^+ and Na^+ diffusion rates and improved electron transport, resulting in outstanding rate performance and cycling stability when employed as anodes in lithium and sodium ion batteries.

The three-dimensional porous architecture inherent to MOF-derived composites significantly facilitates the rapid migration of sodium and potassium ions within electrode materials, thereby accommodating substantial volumetric expansion.[48,104–106] In recent years, these composites have emerged as a focal point of investigation for sodium and potassium ion batteries. The lattice expansion, sluggish reaction kinetics, and low conductivity associated with sodium storage in oxide materials are principal factors that hinder their practical application in SIBs. A judicious adjustment of the compositional structure of oxides presents an effective strategy to modulate their physicochemical properties. Doping heterogeneous atoms within oxides to engender oxygen vacancies and defects has been demonstrated to enhance the intrinsic electron and ion transport rates, thereby improving the sodium storage capacity of these materials.[107,108] For example, Yao et al. synthesized $Mo_{0.1}$–TiO_{2-x}@C with cubic morphologies by doping Mo into Ti-MOF followed by high-temperature calcination.[109] The introduction of Mo ions not only elevated the concentration of Ti^{3+} ions and oxygen vacancies but also resulted in decreased crystallinity, significantly enhancing both the reaction kinetics and sodium storage properties. Specifically, an optimal doping concentration of Mo was found to be advantageous for augmenting electronic conductivity and ion transport rates. $Mo_{0.1}$–TiO_{2-x}@C demonstrates enhanced pseudocapacitance as an anode material in SIBs, reflecting remarkable rate performance and prolonged cycling stability. In addition to metal cation doping, Wang et al. successfully engineered P-doped core–shell NiS_2/C spheres by incorporating phytic acid during the preparation of Ni-MOFs.[110] The incorporation of phosphorus atoms not only increased layer spacing among active materials, facilitating enhanced electron and ion transport, but also introduced anionic defects that modulated the insertion energy of sodium ions, leading to improved electrochemical activity. The expanded layer spacing of NiS_2 expedited the insertion and extraction of Na^+ ions, while the lattice defects generated enriched the active sites, consequently augmenting the conductivity of the ionic crystal structure. This material exhibited an impressive initial reversible discharge capacity of 1113.5 mAh g^{-1} at a current density of 0.1 A g^{-1}, accompanied by excellent rate capability and sustained cycling stability. The development of single-phase bi-anionic metal compounds represents another viable strategy to enhance electrochemical performance. Feng et al. utilized layered Co-MOF as a precursor to synthesize CoPSe/NC with a dual anion structure (Fig. 7d–f).[102] CoPSe possesses intrinsic advantages such as lower mechanical stress, enhanced reaction kinetics, higher theoretical capacity, reduced

discharge voltage, and superior intrinsic conductivity compared to $CoSe_2$ and CoPS. The incorporation of phosphorus atoms leads to an enhanced Na/K storage capacity and reduced reaction stress. Moreover, the synergistic modulation of the electronic structure of the central cobalt atom by selenium and phosphorus optimizes reaction kinetics and lowers the redox potential. The substitution of sulfur atoms with selenium enhances the intrinsic conductivity of CoPSe, thereby effectively suppressing the shuttle effect. Additionally, the unique three-dimensional layered architecture of the CoPSe/NC composite facilitates rapid Na^+/K^+ migration and alleviates the volumetric expansion during cycling, showcasing excellent electrochemical performance when employed as an anode material for sodium and potassium ion batteries. The advantages presented by heterostructures over single-phase compounds have garnered significant attention in the context of potassium ion batteries. Yu et al. achieved commendable potassium storage performance by fabricating hollow Ni_3S_2–Co_9S_8 heterostructures coated with reduced graphene oxide (Fig. 7g–i).[103] The abundant crystalline active interfaces within the Ni_3S_2–Co_9S_8 heterostructures enable rapid charge transfer and notable enhancements in potassium storage performance. The elevated specific surface area of the distinctive open-ended structure further facilitates ion adsorption and migration, thereby improving reaction kinetics. Moreover, the rGO-coated structure effectively mitigates volumetric expansion and particle aggregation during potassium storage. Through the integration of the advantageous characteristics of heterostructures with MOF-derived composite structures, the resultant material exhibited exceptional long-cycle stability, maintaining 348 mAh g^{-1} over 2000 cycles at a current density of 10 A g^{-1}, along with a high energy density of 820 Wh kg^{-1} for the overall battery system.

3.5. Summary

MOF-based materials and their derivatives offer tunable porosity, abundant active sites, and convenient routes to heteroatom-doped carbons and metal compounds, enabling strong lab-scale performance for Li/Na/K-ion batteries. However, translation is hindered by persistent issues: intrinsically low electronic conductivity and framework fragility (poor rate and cycling stability), excessive electrolyte uptake and unstable SEI/CEI formation from very high surface areas, low volumetric density, and scale/cost limitations.

To overcome these gaps, research should focus on linked, actionable priorities: unambiguous mechanistic mapping of ion storage and interphase chemistry using operando/high-resolution probes combined with multiscale modelling; interphase and electrolyte engineering (conformal coatings, tailored electrolytes/additives) to suppress parasitic reactions; architecture-aware synthesis that balances accessible porosity with higher packing density; and intrinsic conductivity or percolating carbon scaffolds plus heterostructured/derivative designs to reconcile capacity, kinetics, and mechanical resilience. Device-relevant metrics (areal capacity, ICE, volumetric energy, full-cell tests) and early attention to scalable, low-cost syntheses are essential.

Short-term work should optimize composites and electrode processing at practical loadings. Mid-term efforts must integrate *operando* diagnostics and modeling to derive transferable design rules. Long-term goals are device-level demonstrations with scalable, sustainable manufacturing. A coordinated push across these fronts—mechanistic science, architecture, interphase control, and scale—will be required to move MOF materials from promising demonstrations to practical, high-energy-density battery components.

4. The applications of MOF and its derivatives for metal–sulfur batteries

The rapid advancement of electric vehicles and electronic devices has underscored the limitations of current commercial LIBs, particularly in terms of energy density, which falls short of the demands for prolonged endurance. Addressing this gap necessitates the development of secondary batteries characterized by high energy density. Sulfur, with its abundant availability, cost-effectiveness, environmental sustainability, and high theoretical specific capacity, has garnered considerable attention in the domain of metal–sulfur battery technology. Various metallic anodes—including Li, Na, K, Al and Ca—are commonly integrated into metal–sulfur battery systems, paving the way for the next generation of secondary batteries that promise reduced costs, extended cycle life, and enhanced energy density. The high theoretical specific capacity of sulfur (1673 mAh g^{-1}) enables diverse metal–sulfur systems to achieve impressive energy densities, such as 2600 Wh kg^{-1} for lithium–sulfur (Li–S), 1273 Wh kg^{-1} for sodium–sulfur (Na–S), and 1023 Wh kg^{-1} for potassium–sulfur (K–S).[111] Nevertheless, despite these remarkable energy densities, several technical challenges persist in metal–sulfur battery systems, which impede their commercial viability. Key challenges include: (1) the multi-electron conversion reactions inherent in metal–sulfur batteries, which lead to the formation of polysulfides (*e.g.*, lithium polysulfide (LiPS), sodium polysulfide (NaPS), and potassium polysulfide (KPS)). The solubility of these polysulfides in ether electrolytes can result in dissolution and shuttling, subsequently causing the loss of reactive sulfur material in the cathode and rapid capacity degradation; (2) the protracted cycling process of the sulfur redox reaction contributes to uneven dissolution and deposition of sulfur, leading to the accumulation of inactive sulfur and sluggish kinetics of the cathodic reaction; (3) the insulating properties of sulfur result in high polarization voltages, slow reaction kinetics, and the necessity for elevated overpotentials, culminating in premature termination of the battery discharge process; (4) the significant volumetric change between sulfur and its final discharge products creates internal stress within the electrode, potentially damaging the structural integrity of the sulfur cathode and adversely impacting long-cycle performance; and (5) the diffusion of soluble polysulfides to the metal anode can initiate side reactions that lead to passivation of the metal electrode and depletion of the electrolyte, further complicating the operational stability of the battery system.

Due to the numerous challenges associated with metal–sulfur battery systems, extensive research has been undertaken in recent years to mitigate various limitations. Key strategies include: (a) incorporating carbon materials to enhance the conductivity of the sulfur anode; (b) introducing active catalytic sites to accelerate the kinetics of sulfur conversion; (c) employing physical limitations and chemical adsorption sites to anchor polysulfides in the cathode, thereby reducing the loss of active material and preventing the passivation of the metal negative electrode due to their dissolution and diffusion; and (d) designing suitable porous materials to accommodate the volume expansion that occurs during the reaction process. Among the range of electrode materials, MOFs emerge as an ideal host for sulfur anodes in metal–sulfur batteries, owing to their high specific surface area, diverse pore structure, and abundance of active sites.[28] A deeper understanding of the mechanisms by which MOF-based materials influence the kinetics of sulfur reactions and enhance stability—through structural design, compositional modulation, and pore structure construction—will significantly contribute to the advancement of next-generation high-energy-density metal–sulfur batteries.

4.1. Pristine MOF

In light of the numerous challenges faced by metal–sulfur battery systems, extensive research has been conducted in recent years to address various limitations. Key strategies include: (a) incorporating carbon materials to improve the conductivity of the sulfur anode; (b) introducing active catalytic sites to enhance the kinetics of sulfur conversion; (c) utilizing physical barriers and chemical adsorption sites to anchor polysulfides within the cathode, thereby minimizing the loss of active material and preventing the passivation of the metal negative electrode caused by dissolution and diffusion; and (d) designing appropriate porous materials to accommodate the volume expansion that occurs during the reaction process. Among the array of electrode materials, MOFs stand out as an ideal host for sulfur anodes in metal–sulfur batteries, thanks to their high specific surface area, diverse pore structures, and rich availability of active sites.[112] A deeper understanding of how MOF-based materials influence the kinetics of sulfur reactions and enhance stability—through structural design, compositional modulation, and pore structure fabrication—will significantly aid in the advancement of next-generation high-energy-density metal–sulfur batteries.

Yuan *et al.* developed a series of multifunctional redox MOFs designed for use as sulfur and lithium anodes in lithium–sulfur batteries.[113] The integration of various Lewis acidic metal clusters (M = Zr^{4+}, Hf^{4+}, and Th^{4+}) alongside redox-active Ni-bis(dithiolene) units (NiS$_4$) in these bifunctional MOF materials significantly enhances both the adsorption strength and catalytic conversion of polysulfides at the cathode (Fig. 8a and b). This results in improved sulfur utilization and mitigation of the shuttle effect. Simultaneously, these materials lower the lithium nucleation barrier, promoting uniform growth and deposition of lithium metal in the anode. Thanks to the remarkable properties of these multifunctional MOFs, a range of advanced M-NiS$_4$ MOF hosts have been developed, leading to
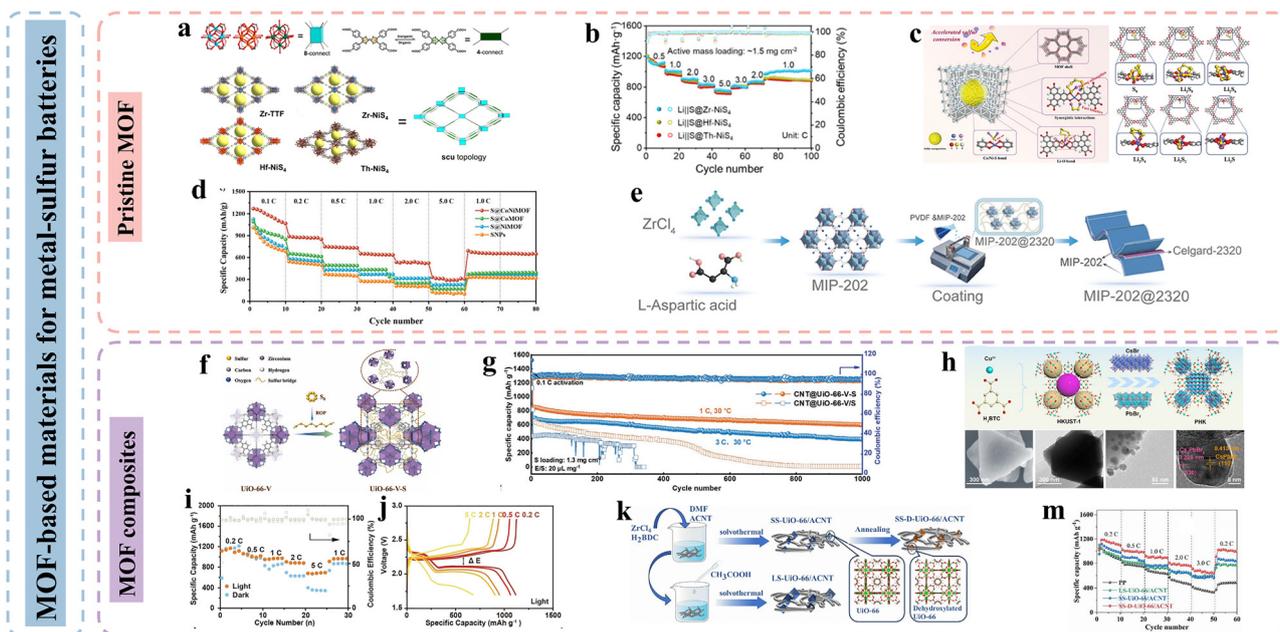
Fig. 8 MOF-based materials for metal–sulfur batteries. (a and b) Various MOF structures and rate performance.[113] Copyright © 2024, Elsevier. (c) Schematic representation of the "fish-in-net" of encapsulated sulfur nanoparticles and polysulfide adsorption models; (d) rate performance.[114] Copyright © 2023, Wiley–VCH. (e) Preparation Process of MIP-202 coated on 2032 separators.[117] Copyright © 2024, Wiley–VCH. (f) The synthesis route of UiO-66-V-S and (g) cycle performance.[118] Copyright © 2022, Wiley–VCH. (h) Schematic illustration of the synthesis of PHK, SEM, TEM, and HRTEM images of PHK; (i) rate performance and (j) charge–discharge curves.[119] Copyright © 2024, Wiley–VCH. (k) Schematic illustration of the preparation stages for UiO-66/ACNT; (m) rate performance.[120] Copyright © 2024, Elsevier.

significantly improved electrochemical kinetics, remarkable capacity retention, and extended cycle life. Lu *et al.* employed a core–shell structural strategy to encapsulate sulfur nanoparticles within a cobalt/nickel bimetal-doped MOF (Fig. 8c and d).[114] This encapsulation achieves spatial confinement of sulfur through its ordered structure while providing abundant chemically active sites. The outer layer of the core–shell structure ensures a uniform encapsulation of internal polysulfides, effectively inhibiting the dissolution of lithium polysulfides in ether-based electrolytes. Furthermore, the metal–sulfur (M–S) coordination bond and covalent bonding play a crucial role in polysulfide adsorption. Notably, delocalized electrons around the metal ions in the designed MOFs facilitate electron and ion transport, thereby enhancing the electrical conductivity of the anode. These advantages contribute to the effectiveness of the proposed "fish-in-net" strategy, which exhibits improved interfacial charge transfer kinetics, a heightened sulfur redox rate, and effective suppression of the shuttle effect when utilized as a cathode in lithium–sulfur batteries.

The iron-based MOF (MIL-100 (Fe)) has proven effective in stabilizing the long-cycle performance of metal–sulfur batteries.[115] Its unique chemical and morphological properties, combined with structural advantages, allow it to act as an anchor for polysulfides within microporous cathode materials. The framework of MIL-100 (Fe) is constructed from oxo-centered trinuclear Fe(III) clusters and 1,3,5-benzenetricarboxylate (BTC^{3-}) as the ligand, featuring pore sizes of approximately 5 Å and 8.6 Å. This design facilitates the efficient embedding of S8 (6.88 Å) and polysulfide within its structure. The tailored confinement strategy

enabled by this porous framework demonstrates exceptional cycling stability for S@MIL-100(Fe) composites when utilized as sulfur hosts in lithium/sodium–sulfur batteries. Exploring the mechanisms and achieving a deeper understanding of polysulfide confinement is crucial for minimizing polysulfide shuttling. Qiao *et al.* proposed a novel mechanism for effective polysulfide confinement based on a 2D Ni-MOF.[116] The electronic state of the metal nickel within the MOF has been shown to enhance the regulation of the adsorption strength of sodium polysulfide, thereby improving the suppression of the shuttle effect and accelerating reaction conversion kinetics. Additionally, the study analyzes the relationship between the localized electronic state of sulfur and the kinetics of polysulfide conversion. This comprehensive understanding of polysulfide adsorption and conversion mechanisms contributes significantly to developing highly stable metal–sulfur batteries.

Despite the advantages of high specific surface area and abundant active sites, pristine MOFs have primarily been explored for use in Li–S batteries, with comparatively few studies focusing on Na- or K–sulfur batteries and other types. Investigating the exceptional catalytic activity of pristine MOFs and their effects on the catalytic and adsorptive processes in other metal–sulfur batteries has the potential to expand the application range of these materials, thereby facilitating the development of higher-performance batteries.

In addition to serving as a sulfur anode host, pristine MOFs have been utilized in the development of separators and intercalation materials for lithium–sulfur batteries. MOF materials are characterized by their highly efficient capabilities for

polysulfide interception and conversion, as well as rapid lithium ion conduction, which collectively facilitates the performance optimization of lithium–sulfur battery systems.[121,122] Zhang et al. engineered composite separators incorporating MIP-202 (Zr)-modified Celgard-2320 utilizing a double-sided coating strategy to enhance the functionality of lithium–sulfur batteries (Fig. 8e).[117] The polar ligand and porous architecture of MIP-202 (Zr) demonstrated superior adsorption properties for lithium polysulfides, coupled with enhanced electrolyte permeability. Additionally, its sub-nanoporous structure exhibited substantial Li+ passivity alongside physical constraints on lithium polysulfide migration, effectively alleviating the notorious shuttle effect. The synthesis process generates a negative electron cloud within the channel due to the presence of Cl− ions, which further accelerates the migration rate of Li+ while impeding the diffusion of lithium polysulfides towards the negative electrode. This phenomenon endows the composite separator with noteworthy flame-retardant characteristics. In contrast to crystalline MOFs, the disordered structure and abundant defect sites inherent in amorphous MOF materials confer advantages for catalytic polysulfide conversion, owing to the random coordination of ligands and metal ion clusters present in amorphous MOFs, which are characterized by ligand defects and a high specific surface area with a diverse pore size distribution. Bi et al. pioneered the synthesis of amorphous bimetallic MOF materials featuring ligand defects (aFeNi-MOF) through a ligand competition strategy aimed at modifying separators.[123] This approach not only facilitated enhanced ionic migration but also elevated the chemisorption and catalytic efficacy of sulfur species. Furthermore, the substantial number of unsaturated metal sites resulting from ligand removal is anticipated to serve as active sites for accelerating the kinetics associated with sulfur processes, effectively suppressing the shuttle effect. The aFeNi-MOF-modified separators demonstrated exemplary cycling stability and capacity retention in lithium–sulfur battery applications. Chen et al. synthesized Zn–Co bimetallic MOFs (D-ZIF L) through undercoordination modification, achieved by the selective removal of organic ligands from the active center.[124] Such ligand deficiency fosters full interaction between the metal active center and sulfur species, thus significantly enhancing the catalytic efficiency of the MOF. Additionally, the defects arising from the redistribution of electronic states in the undercoordinated active metal centers, induced by the elimination of organic ligands, contribute to an increased electron density at the Fermi energy level. This manipulation results in the tuning of intrinsic conductivity within pristine MOFs and strengthens the adsorption interactions with polysulfides. Consequently, based on the underlying chemical mechanisms associated with undercoordination, the synthesis of highly conductive MOFs is anticipated to expand the applicability of pristine MOF materials in metal–sulfur battery technologies.

4.2. Composite MOF and functional materials

The incorporation of MOFs in the domain of metal–sulfur batteries has garnered significant attention due to their abundant metal active centers and porous structures, which effectively catalyze the transformation of polysulfides while mitigating shuttle effects. Nonetheless, the inherent limitation of MOFs regarding electrical conductivity remains a critical challenge that constrains their application in this field. Recent studies have elucidated that complexes formed from pristine MOF materials can enhance conductivity and synergistically improve polysulfide adsorption strength alongside catalytic conversion efficiency. For instance, Li et al. synthesized a free-standing sulfur electrode by integrating copper into r-GO in the form of MOF particles.[125] The introduction of copper imparted several noteworthy advantages to the complexes, including: (1) an increased presence of sp2-hybridized carbon, which significantly enhances the electron transport rate and minimizes the overpotential associated with sulfur reactions; (2) improved adsorption strength and confinement of lithium polysulfides, which effectively mitigates the shuttle effect; and (3) a notable acceleration of the kinetics associated with the sulfur redox reaction, thereby enhancing the electrochemical performance of the battery. Leveraging these structural attributes and improved conductivity, the modified materials continue to demonstrate exceptional electrochemical performance even under extreme operational conditions when utilized as cathode hosts in lithium–sulfur batteries.

Furthermore, Wang et al. demonstrated the enhancement of electrical conductivity by coupling multi-walled carbon nanotubes with indium-based MOFs.[126] This hybrid material not only bolstered conductivity but also capitalized on the Lewis acidic characteristics of indium-based MOFs. Consequently, the material exhibited favorable effects in reducing shuttle effects and effectively confining short-chain lithium polysulfides (Li_2S_2 and Li_2S_4, with dimensions <2 nm) within the micropores of the MOF due to its optimal pore structure and chemical properties; additionally, the robust In–S bonding significantly mitigated the loss of reactive sulfur species, thereby enhancing the stability of lithium–sulfur batteries. Beyond the amalgamation of MOFs with conductive materials, the functionalization of MOF materials emerges as a potent strategy to improve the kinetics for sulfur reactions. Huang et al. synthesized a MOF-sulfur copolymer (CNT@UiO-66-V-S) by integrating sulfur with vinyl-functionalized MOFs (Fig. 8f and g).[118] The reaction mechanism was elucidated through in situ Raman spectroscopy, revealing the role of free radicals in catalyzing lithium polysulfide conversion. The findings indicated that vinyl radicals actively accelerate this conversion process while inhibiting the growth of lithium dendrites at the negative electrode. This co-polymerization strategy enabled lithium–sulfur batteries to achieve remarkable discharge capacities and long-cycle stability, presenting a promising avenue for the development of functionalized MOF materials intended for electrochemical energy storage. Despite advancements in traditional physical confinement, chemical adsorption, and electrochemical catalysis, there remain inherent limitations in reducing the liquid–solid reaction energy barriers.[127] In a novel approach, Chen et al. developed a light-assisted lithium–sulfur battery system that generates a built-in electric field at the micro-interface, thereby

prolonging the lifetime of photogenerated carriers.[119] By constructing a heterostructure consisting of $CsPbBr_3/Cs_4PbBr_6$ perovskite quantum dots modified MOF (HKUST-1), which facilitates spatial constraining effects, the generated electron–hole pairs under light-assisted conditions enable precise regulation of polysulfides (Fig. 8h–j). This innovative approach not only leads to a substantial enhancement in capacity for lithium–sulfur batteries, but the electron–hole pairs also reduce the redox potential of sulfur species during the catalytic process, thereby accelerating liquid–solid conversion efficiency and enhancing sulfur utilization to achieve superior electrochemical performance.

MOFs present distinctive advantages in the modification of separators and the design of intercalation systems for lithium–sulfur batteries. The introduction of active materials between the cathode and separator can effectively impede the shuttle effect of lithium polysulfides while mitigating side reactions associated with lithium metal. Specifically, the unique narrow pore structure of MOF-801(Zr), a result of its –OH functional groups and structural defects within the Zr oxo-cluster, offers significant benefits for the physical confinement and chemical adsorption of lithium polysulfides. Recent work by Lu et al. highlights the development of a flexible, free-standing MOF-based intercalation layer characterized by superior mechanical strength and chemical stability.[128] The densely packed pore architecture of MOF-801, combined with the exposure of Zr–OH active sites, facilitates effective anchoring of lithium polysulfides while enhancing lithium ion transport. Furthermore, the incorporation of conductive carbon not only increases overall conductivity but also promotes the reactivation of sulfur species within the MOF pores. The resultant composite intercalated diaphragm demonstrates exceptional chemical performance within lithium–sulfur battery applications. The UiO-66 family of MOFs, featuring coordinated $Zr_6O_4(OH)_4$ octahedral clusters, exhibits Lewis acidity and a robust anchoring capability for polysulfide anions (S_n^{2-}, $4 \leq n \leq 8$), thereby enhancing Li^+ conduction.[129,130] In a notable contribution by Li et al., a synergistic structural and electronic tuning approach was employed to construct a composite system (UiO-66/ACNT) that combines small-sized dehydroxylated UiO-66—enriched with active sites—and acid-treated carbon nanotubes (ACNT) (Fig. 8k–m).[120] The particle size of UiO-66 was effectively optimized by introducing acids as modifiers, resulting in a small-particle dehydroxylated UiO-66 linked by ACNT, which exhibits remarkable conductivity. This innovative small-size strategy fosters abundant Lewis acidic interactions, which in turn facilitate strong anchoring of lithium polysulfides. Moreover, the exposed Zr sites and one-dimensional electron transport pathways greatly accelerate the kinetics of sulfur reactions. The composite demonstrates exceptional cycling stability, exhibiting only 0.06% capacity degradation per cycle at 1C over 1000 cycles, while achieving a high area capacity of 4.01 mAh cm^{-2} at 0.2C when implemented as a separator in lithium–sulfur batteries.

4.3. MOF derivatives carbon-based materials

The insulating properties of sulfur significantly hinder its electrochemical performance, resulting in substantial voltage polarization and slow reaction kinetics during both charging and discharging. Additionally, the low conductivity of pristine MOFs imposes further limitations for their direct application in metal–sulfur batteries. In contrast, the characteristics of MOF-derived carbon materials—including their high specific surface area, elevated porosity, abundant active sites, and excellent conductivity—facilitate the uniform distribution of sulfur within the cathode and enhance electrical conductivity. As such, these materials are regarded as ideal hosts for anode sulfur in metal–sulfur batteries.

Jiang et al. used ZIF-8 nanosheets as precursors to prepare hierarchical porous carbon structures with two-dimensional sheet-like structures (Fig. 9a). The two-dimensional planar "plane to plane" pattern constructs an effective conductive network, which promotes fast electron transport and reaction kinetics. In addition, the high specific surface area and hierarchical pore structure enable the sulfur to be uniformly embedded in the main body and effectively alleviate the volume expansion during the reaction process; the nitrogen doping property introduced by organic ligands also endows the carbon main body with excellent adsorption of lithium polysulfide, which realizes the excellent cyclic stability.[131] The excellent conductivity of porous carbon materials facilitates rapid electron transport and accelerates the redox kinetic process; however, carbon materials are weak in adsorption and anchoring of lithium polysulfide. Functionalized porous carbon is an effective strategy to inhibit the shuttle effect.[132] Fang et al. fluorine-doped ZIF-8-derived carbon material and used as a modification material for the lithium–sulfur battery separator.[133] Based on retaining the original polyhedral structure, the introduced F atoms of the ZIF-8-derived carbon materials not only play a modulating role in the electronic conductivity, but also the highly polar carbon rings generated by the N, F co-doping strategy of the polar character show strong adsorption strength for lithium polysulfide, which is conducive to the suppression of the shuttle effect and the enhancement of the sulfur utilization rate.

The anchoring effect of MOF-derived carbon materials on polysulfides is acknowledged; however, the sluggish conversion kinetics of polysulfides remain a critical challenge in the development of metal–sulfur batteries. The presence of metal nanoparticles, metal compounds, and metal single atoms plays a crucial role in accelerating sulfur species reaction kinetics. MOF materials, characterized by their metal centers and organic ligands, transform carbon materials and metal compounds during high-temperature treatment. The resulting active metal centers can serve a catalytic function in reactions involving sulfur species, while also fulfilling requirements for high porosity and electrical conductivity. In their study, Song et al. synthesized porous hard carbon materials containing cobalt nanoparticles (Co-NP) through an ultrafast high-temperature sintering technique applied to ZIF-67.[134] The 3D electron tomography confirmed the ultra-small size and uniform dispersion of Co nanoparticles within carbon nanocages. The unique properties of small size, uniform distribution, and the catalytic effects attributed to the confinement of Co
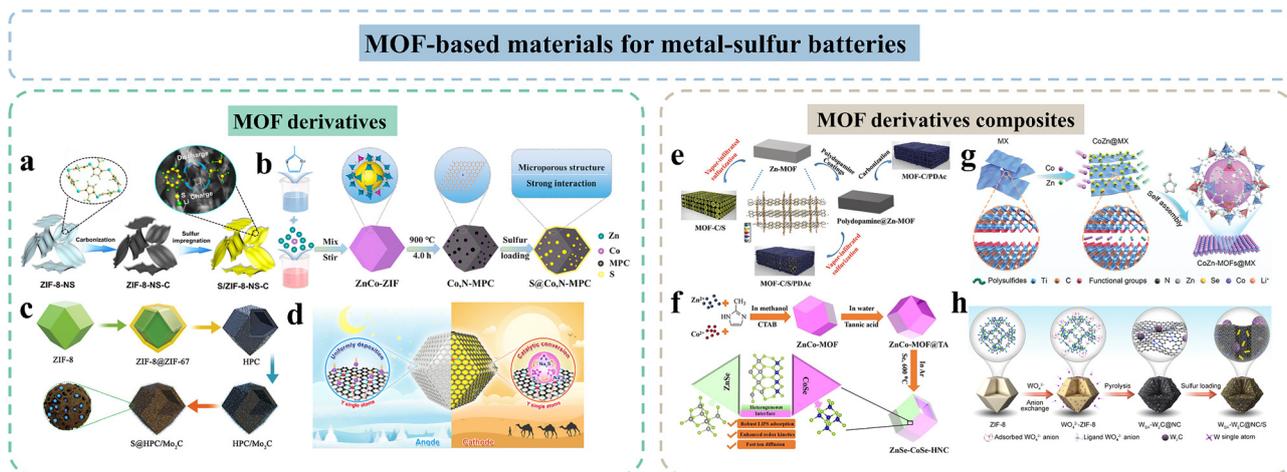
Fig. 9 MOF-based materials for metal–sulfur batteries. (a) The preparation route of S/ZIF-8-NS-C composites.[131] Copyright © 2017, American Chemical Society. (b) The preparation process of S@Co, N-MPC composites.[136] Copyright © 2023, Elsevier. (c) The preparation of the S@HPC/Mo$_2$C.[138] Copyright © 2022, Wiley–VCH. (d) Schematic illustration of yttrium single atom for sodium–sulfur battery full cell.[139] Copyright © 2022, American Chemical Society. (e) Fabrication process of MOF-C/S/PDAc composites.[140] Copyright © 2022, Wiley–VCH. (f) The synthesis of ZnSe-CoSe-HNC.[141] Copyright 2023, Elsevier. (g) Synthesis process and structure of CoZn-Se@N-MX.[52] Copyright © 2021, Wiley–VCH. (h) Schematic synthesis process of W$_{SA}$–W$_2$C@NC and W$_{SA}$–W$_2$C@NC/S.[142] Copyright 2024, Nature Publishing Group.

nanoparticles within the nanocages contribute to enhanced electrochemical performance in lithium–sulfur batteries. Furthermore, Liu *et al.* reported the preparation of a structure comprising graphitized carbon shells encapsulating nickel nanoparticle cores *via* one-step thermal polymerization of Ni-MOF.[135] The nickel particles are effective in capturing lithium polysulfide generated during the charge–discharge cycles, thereby mitigating the diffusion of lithium polysulfide to the outer shell. Additionally, the graphitized carbon-coated nickel particles act as active centers, offering numerous active sites that facilitate the rapid conversion of lithium polysulfides, thereby reducing voltage polarization and enhancing both the reaction kinetics and cycling stability of lithium–sulfur batteries. Jin *et al.* developed a nitrogen-doped microporous carbon matrix (Co, N-MPC) embedded with cobalt nanoparticles (Fig. 9b), utilizing CoZn-ZIFs as precursors.[136] Their findings indicate that the optimization of metal ratios within the carbon matrix maximizes the adsorption capacity for sulfur species. The incorporation of cobalt nanoparticles within a microporous carbon matrix, alongside nitrogen doping, effectively accelerates the kinetics of sodium polysulfide conversion through strong interactions with sodium polysulfides. The microporous structure not only facilitates efficient electron transfer for sulfur but also stabilizes the volumetric changes associated with sulfur. To harness the catalytic potential of metal nano-ions fully, Ge *et al.* prepared porous nitrogen-doped carbon embedded with n-doped cobalt nanoclusters derived from ZIF-67 using a straightforward low-temperature thermal polymerization method.[137] The resultant cobalt nanoparticles exhibited tunable sizes, ranging from 7 nm to uniform clusters of 3 nm, thus presenting a greater availability of active sites for polysulfide adsorption. The dispersed active sites significantly enhance the conversion kinetics of lithium polysulfide to the ultimate discharge products while effectively suppressing the

shuttle effect. The developed S–N–Co$_s$–C cathode, featuring 3 nm cobalt clusters, demonstrates exceptional catalytic activity, reduced charge transfer resistance and energy barriers, elevated exchange current density, and an accelerated conversion reaction rate, thereby underscoring its potential in potassium–sulfur battery applications.

Metal compounds are known for their robust adsorption strength and remarkable catalytic performance concerning polysulfides, particularly when compared to the significant polarity characteristics inherent to metal clusters. In their research, Xie *et al.* synthesized N-doped carbon nanosheet arrays, designated as Co$_{0.85}$Se/NC, which incorporated Co$_{0.85}$Se nanoparticles as self-supported sulfur cathodes.[143] This was achieved through the growth of a cobalt Co-MOF on carbon cloth, followed by a high-temperature treatment process. The resulting interconnected porous carbon structure facilitates rapid electron migration and ion transport, while the Co$_{0.85}$Se component exhibits excellent trapping capabilities and catalytic activity for lithium polysulfides. This dual functionality enhances the sulfur redox kinetics and stabilizes the sulfur anode. Further advancing this area, Yao *et al.* developed an N-doped hollow carbon composite (CoS/HNC), which contained well-dispersed CoS nanoparticles derived from the carbonization of functionalized MOFs.[144] The synthesis process involved a non-homogeneous growth of UiO-66-NH$_2$, which led to a high density of defective sites within the core and resulted in a hollow structure *via* selective etching. The CoS/HNC complexes effectively mitigate volume expansion and provide catalytic anchoring for lithium polysulfides through the polar CoS component. The utilization of dispersed active sites within the MOF derivatives ensures that the passivation of catalytic sites during the reaction is minimized, thus allowing for sustained catalytic activity that yields excellent electrochemical performance in lithium–sulfur batteries. Additionally, Yu *et al.*

prepared hollow porous carbon embedded with Mo_2C particles (designated as HPC/Mo_2C) using ZIF-8 as a precursor template, targeting sulfur hosting in room-temperature sodium–sulfur batteries (Fig. 9c).[138] The resultant micro- and mesoporous hollow carbon enhanced both reactivity and accommodated the volume expansion associated with the sulfur positive electrode. The highly conductive HPC plays a crucial role in regulating electrode conductivity and reducing voltage polarization during charge–discharge cycles. Moreover, the dispersed Mo_2C particles exhibit strong chemical adsorption capacity for polysulfides and catalyze their conversion, effectively inhibiting solubility issues related to polysulfides and accelerating reaction kinetics. Consequently, the S@HPC/Mo_2C cathode demonstrates high discharge specific capacity and superior rate performance, affirming its potential in energy storage applications.

Single-atom catalysts (SACs) have emerged as a prominent area of research within the realm of energy catalysis in recent years, owing to their remarkable atomic utilization, distinctive physicochemical properties, and superior catalytic performance. The ordered MOF nodes are particularly advantageous because they are more likely to retain their original metal-site distribution structure after high-temperature carbonization. This results in exceptional specific surface areas, intricate pore structures, and tunable surface properties, all of which are beneficial for the fabrication of SAC materials.[145,146] The application of SACs to enhance the conversion kinetics of polysulfides represents a significant advancement in this field. For instance, Li et al. successfully synthesized N-doped carbon (Co-SAs@NC) integrated with cobalt single-atom sites via high-temperature pyrolysis, utilizing CoZn-ZIF as a precursor.[147] Given that Zn-ZIF and Co-ZIF share identical topological frameworks, the preparation of binary Zn–Co ZIF precursors utilizing bimetallic ions effectively mitigates the aggregation of monometallic cobalt. Following high-temperature treatment and the subsequent removal of zinc, dispersed cobalt sites are generated, yielding cobalt single atoms endowed with an N-coordinated structure that exhibits strong adsorption affinity for lithium polysulfide alongside excellent catalytic kinetics. The potential of MOF materials in modulating catalytic single-atom sites and facilitating hybridization with guest molecular orbitals provides valuable insights into their catalytic mechanisms in lithium–sulfur batteries, guiding the development of highly efficient SACs. Huang et al. designed and synthesized a range of porphyrin-based MOF nanosheets, denoted as PCN-222(M)-NSs (where M = Fe^{3+}, Co^{2+}, Ni^{2+}, and Cu^{2+}), and systematically examined the catalytic mechanisms underlying the sulfur redox processes catalyzed by different single-atom catalysts.[148] Notably, the orbital hybridization occurring between the M–N_4 sites and sulfur species was identified as a critical factor in enhancing the catalysis of lithium polysulfide. PCN-222(Cu)-NS demonstrates optimal catalytic behavior in the sulfur redox reaction (SRR) due to its more efficient d–p orbital hybridization. This phenomenon is characterized by stronger interactions with lithium polysulfide and a reduction in the potential barrier associated with the Li_2S oxidation process. The intrinsic mechanisms by which SACs

suppress the shuttle effect and accelerate the SRR process have been substantiated.

In contrast to the varied d-bands of transition metals, the abundant electronic structure of the 4f orbitals of rare earth metals confers a strong adsorption capacity for reactant molecules, albeit with diminished activity in room-temperature electrochemical reactions.[149] The engineering of single-atom coordination structures in rare-earth metals has been shown to stimulate spin–orbital interactions, thereby enhancing catalytic activity effectively.[150] For example, Li et al. employed theoretical predictions to fabricate single-atom hybrids using MOF as a precursor, successfully doping yttrium (Y) single atoms into nitrogen-doped orthorhombic carbon structures (Y SAs/NC) (Fig. 9d).[139] The incorporation of single-atom Y exhibited exceptional sodiophilicity and sulfiphilicity, catalyzing the reduction of S_8 to the final discharge product Na_2S. This process not only accelerates reaction kinetics and alleviates the shuttle effect but also promotes uniform plating/stripping of sodium when utilized as a sodium-negative electrode host. The Y SAs/NC demonstrated impressive electrochemical performance when integrated into sodium–sulfur full batteries. Typically, the loading of single atoms is maintained within the range of 1–5%, as increased loading often leads to the aggregation of metal atoms, which detracts from their electrocatalytic activity. Therefore, there is an urgent need to explore novel methodologies for achieving high-loading single atoms.[151] Xiao et al. addressed this challenge by synthesizing an N, O co-doped carbon-loaded copper single-atom substrate (Cu SA/NOC) using a bimetallic (Cu, Zn) MOF precursor.[152] Following the removal of the Zn component through chemical treatment, well-dispersed Cu single-atom sites (approximately 0.2 nm) with loading as high as 8% were obtained. These Cu single-atom sites demonstrated a capability to weaken the S–S bond within the S_8 ring, facilitating the generation of short-chain sulfur molecules while simultaneously hindering the formation of polysulfide intermediates. The robust catalytic properties of Cu single atoms significantly accelerated electrochemical reaction kinetics, enhanced the conversion of sulfur to Na_2S, and improved sulfur utilization and rate performance by promoting the diffusion rate of Na^+. The impressive single-atom loading achieved through this method underscores the inherent advantages of MOF-derived SACs, paving the way for the design of highly efficient electrocatalysts.

4.4. MOF derivative composite with functional materials

Although MOF derivatives display remarkable properties in the adsorption and catalytic kinetic reactions of polysulfides, the discontinuity among the original MOF-derived particles hampers rapid electron transport. Therefore, creating a specialized structure to establish an electron transport network between the MOF-derived particles is essential for further enhancing the electrochemical properties of these derivatives.

Wu et al. synthesized hollow polyhedral carbon functionalized with CNTs to serve as an anode host for lithium–sulfur batteries through the etching and low-temperature treatment of ZIF-8.[153] This scaffold exhibits an ordered hollow structure and a conductive network; the incorporation of heteroatoms and

the hydrophilic nature of the surface contribute to enhanced adsorption strength of lithium polysulfides. Additionally, these features facilitate the kinetic acceleration of sulfur reactions and modulate the deposition behavior of the discharge product, Li_2S. The strategy employed in developing this MOF-derived composite effectively combines the porous structural characteristics of MOF-derived carbon materials with the superior electrical conductivity afforded by the functionalized CNTs, resulting in outstanding electrochemical performance as cathode hosts for lithium–sulfur batteries. Ding et al. introduced a methodology for constructing 2D hetero-structured carbon nanosheets integrated with a 3D porous carbon framework (PCF) via the wrapping of GO around ZIF-8.[154] Within this framework, the MOF particles served as precursor materials that not only allowed for precise control over the size and morphology of the synthesized materials but also facilitated the incorporation of nitrogen-containing organic ligands from ZIF-8, leading to the production of nitrogen-doped carbon. The resultant PCF materials demonstrated a high surface area and substantial pore volume, making them ideal hosts for sulfur cathodes in lithium–sulfur batteries. Notably, the PCF/S composite exhibited a high specific discharge capacity and remarkable cycling stability. In a separate investigation, Xiao et al. prepared zinc-based MOF materials utilizing a solvothermal method, employing 2,5-thiophenedicarboxylic acid and 1,4-bis(pyrid-4-yl) benzene as ligands. These materials were subsequently encapsulated with polydopamine (PDA)-derivatized nitrogen-doped carbon, resulting in the formation of porous tubular carbon structures with homogeneous sulfur and nitrogen co-doping, characterized by tubular apertures ranging from approximately 1.5 nm to 0.8 nm (Fig. 9e).[140] These structures were effectively utilized for sulfur storage through a vapor-infiltration technique, wherein the formation of $C–S_x–C$ bonds ensured a uniform dispersion and binding of sulfur. Furthermore, the outer N-doped carbon layer significantly enhanced the sulfur content within the composite, achieving elevated sulfur loading and ensuring high sulfur utilization, thereby mitigating the shuttle effect inherent in sodium–sulfur batteries.

In addition to the extensive research on MOF-derived carbon complexes, considerable attention has been devoted to MOF-derived carbon/metal compound complexes. Feng et al. synthesized a hollow N-doped carbon nanocage (ZnSe–CoSe–HNC) featuring embedded heterostructures of ZnSe–CoSe nanoparticles using a ZIF as a precursor (Fig. 9f).[141] The hollow architecture of this material facilitates considerable internal space for sulfur accommodation while simultaneously addressing volume expansion issues. The enriched heterogeneous interface of ZnSe–CoSe significantly enhances reaction kinetics and mitigates the shuttle effect, serving as a bifunctional active center for both adsorption and catalysis. Coupled with the superior electrical conductivity of the resulting carbon matrix, the ZnSe–CoSe-HNC/S cathode demonstrates exceptional electrochemical performance. Moreover, the construction of multimetallic heterostructures presents distinct advantages over monometallic MOF derivatives, effectively improving the electrochemical characteristics of lithium–sulfur batteries.

For instance, Chu et al. developed $CoSe_2/Co_3O_4$ heterostructures encapsulated by nitrogen-doped carbon layers and carbon nanotube frameworks (NC-CNT) through a coaxial self-templated growth method, utilizing ZIF-67 coated on ZIF-8.[155] The synergistic interactions among the conductive channels, the electrolyte, and the adsorption-catalysis three-phase interfaces culminate in enhanced electron transport rates, improved bonding to lithium polysulfide, and heightened catalytic activity. This intricate architecture substantially modulates the reaction kinetics of soluble lithium polysulfide, promoting a uniform dissolution and deposition of Li_2S. Within the diverse $CoSe_2/Co_3O_4$ heterostructures, Co_3O_4 demonstrates a significant adsorption capacity for lithium polysulfide, expediting the conversion reaction by facilitating diffusion into the $CoSe_2$ interface. The highly conductive NC-CNT network is particularly advantageous in accelerating the reaction kinetics, while the sulfur-rich active sites of the $CoSe_2/Co_3O_4$ heterostructures foster the consistent precipitation of Li_2S. Consequently, the $CoSe_2/Co_3O_4$@NC-CNT/S anode, sculpted by the aforementioned structural benefits, exhibits remarkable electrochemical performance.

Additionally, the integration of MOF derivatives with 2D materials for constructing 0D–2D heterogeneous electrocatalysts emerges as an effective strategy to mitigate the discontinuity inherent in MOF particles. Chen et al. employed MXene as a substrate and uniformly produced CoZn bimetallic MOF particles on its surface, resulting in bimetallic selenide/N-doped MXene (CoZn–Se@N-MX) complexes featuring a 0D–2D structure through high-temperature treatment (Fig. 9g).[52] The resultant hybrid architecture, composed of 0D CoZn–Se nanoparticles and 2D N-MX nanosheets, yields amphiphilic lithium–sulfur sites that effectively immobilize and catalyze the conversion of lithium polysulfide. The hierarchical porous framework inherent to this design provides a substantial surface area, facilitating rapid Li^+ transport. Importantly, the combination of MOF-derived particles with 2D materials adeptly mitigates particle accumulation and promotes enhanced catalytic activity. Furthermore, Yu et al. investigated the composite of ZIF-67-derived Co_3Se_4@N–C with $Ti_3C_2T_x$ for the modification of polypropylene (PP) separators via electrostatic adsorption.[45] This innovative design capitalizes on the synergistic effects inherent in the combination of the exceptional catalytic performance of Co_3Se_4@N–C with the enhanced adsorption capabilities and electrical conductivity of $Ti_3C_2T_x$. The outcome is an acceleration of the kinetic rates associated with lithium polysulfide conversion reactions while effectively constraining the shuttle effect. Overall, this design harmoniously merges the advantages of catalysis and adsorption, thereby contributing to the advancement of lithium–sulfur batteries with commendable electrochemical performance.

The two-site design of MOFs that are derived in situ to create metal single atom/metal composite structures demonstrates remarkable electrocatalytic performance. Zhao et al. utilized 3D polystyrene nanospheres as soft templates, facilitating the growth and high-temperature treatment of CoZn-MOF in the interstitial spaces.[156] This process resulted in the embedding of ZnS nanoparticles and Co–N–C single-atom catalysts to form

double-end binding sites within a macroporous carbon skeleton. During the cycling process, the polysulfide intermediates were effectively immobilized and catalytically converted, thereby eliminating the shuttle effect and mitigating the corrosion of lithium metal. Additionally, the three interfaces formed among the catalyst, conductive support, and electrolyte within the ordered macroporous carbon network enhance electron transfer and the rapid transport of Li$^+$, preventing the generation of inactive sulfur. In a separate study, Song et al. established two coordination environments for tungsten atoms within the MOF framework, leading to the formation of tungsten single atoms and tungsten carbide nanocrystals (W_{SA}–W_2C@NC) during high-temperature calcination (Fig. 9h). These materials were employed to optimize the kinetics of potassium polysulfides, thereby facilitating the construction of high-performance potassium–sulfur batteries.[142] The tungsten carbide serves as a catalytic site for potassium polysulfides, expediting the sulfur reaction kinetics, while the tungsten single atoms enhance the polysulfide migration rate, significantly alleviating the accumulation of insulating sulfides and the associated catalytic poisoning.

4.5. Summary

Pristine MOFs and their derivatives show strong promise as sulfur hosts and catalysts in metal–sulfur batteries, thanks to tunable metal active centers, rich pore networks, and tailored ligand chemistry. However, their practical use is limited by intrinsically low electronic conductivity, particle aggregation, and the low packing density of many MOF-derived particles—factors that hinder electron access to internal sulfur and reduce sulfur utilization. Minimizing ion–electron diffusion distances through morphology control (high-aspect-ratio 1D scaffolds, 2D nano-flakes, or densely packed 3D nano-particles) is therefore essential to improve internal charge transport and reaction completeness.

Composite and derivative strategies are the most effective routes forward: engineering continuous 3D conductive networks (in situ carbon, CNT/graphene scaffolds, or conductive coatings) accelerates sulfur redox kinetics, while controlled pyrolysis and deliberate ligand selection produce highly conductive, heteroatom-doped carbon matrices. Equally important is the spatial tuning of metal active sites—uniform dispersion, heterojunction formation (metal/metal-compound interfaces), multisite catalysis, and 0D–2D architectures all strengthen polysulfide adsorption and speed catalytic conversion. Future work should focus on quantifying these synergies with operando diagnostics and standardized device-level metrics to translate promising materials into durable, high-utilization metal–sulfur cells.

5. The applications of MOF and its derivatives for zinc-ion batteries

Aqueous zinc ion batteries (ZIBs) are considered promising candidates for next-generation energy storage solutions due to their high theoretical capacity (820 mAh g^{-1}), affordability, enhanced safety, and environmental friendliness.[157,158] However, various challenges associated with the positive electrode, negative electrode, and electrolyte still hinder their commercial viability. Current cathode materials used in zinc ion batteries include manganese-based oxides, vanadium-based oxides, Prussian blue analogs, and organic materials. The slow diffusion rate of Zn^{2+} ions and the irreversible phase transitions in manganese-based materials during cycling contribute to poor cycling stability and capacity degradation. Additionally, the lower voltage and toxicity associated with the high-valent vanadium in vanadium-based materials restrict their application. Although Prussian blue offers a high voltage (1.6–1.8 V), it suffers from low capacity. Organic materials exhibit a high theoretical specific capacity; however, their poor electrical conductivity and low practical capacity still limit their commercialization. For the zinc negative electrodes, while zinc foils demonstrate excellent stability under air and moisture conditions, the repetitive dissolution and deposition of Zn^{2+} ions during complex electrochemical reactions can result in the formation of insoluble negative dendrites on the surface of the electrodes. This inhomogeneous deposition can lead to accumulation on the surface, causing rapid capacity decay and reduced coulombic efficiency. Given the multifunctionality of MOFs, with their abundant pore structures and active sites, these materials have garnered extensive attention and have made significant advancements in zinc ion battery applications.

5.1. Pristine MOF

Due to their rich pore structure, diverse functional properties, and controllable morphology, pristine MOF materials offer distinct advantages for ZIBs. However, the existing vanadium-based cathode materials primarily consist of vanadium compounds, making it relatively challenging to develop vanadium-based MOF materials suitable for direct application in ZIBs.

Mondal et al. successfully synthesized MIL-100 (V), a MOF characterized by a highly porous structure, which was employed as a cathode material for ZIBs via a hydrothermal method.[159] This MOF exhibits an exceptionally high specific surface area of 2320 m^2 g^{-1} and mesoporous channels, which facilitate the insertion and extraction of Zn^{2+} ions. The robust framework structure contributes significant stability when immersed in electrolyte solutions. Moreover, the presence of V^{2+}/V^{5+} redox pairs within MIL-100 (V) enhances the discharge capacity, while the V–O bonds in the MOF system serve a dual purpose: they effectively inhibit the dissolution of the cathode material and improve the structural stability during charge/discharge cycles. Consequently, MIL-100 (V) achieves a remarkable specific capacity of 362 mAh g^{-1}, demonstrating substantial stability and energy density over 3500 cycles. In response to the limitations of MOF materials, particularly their low capacity and suboptimal cycling performance, Xu et al. developed an innovative organic/inorganic dual electrochemically active site manganese-based MOF (Mn-MOF-74). This framework is engineered to enhance overall capacity and energy density (Fig. 10a). The Mn-MOF-74 cathode operates through two distinct
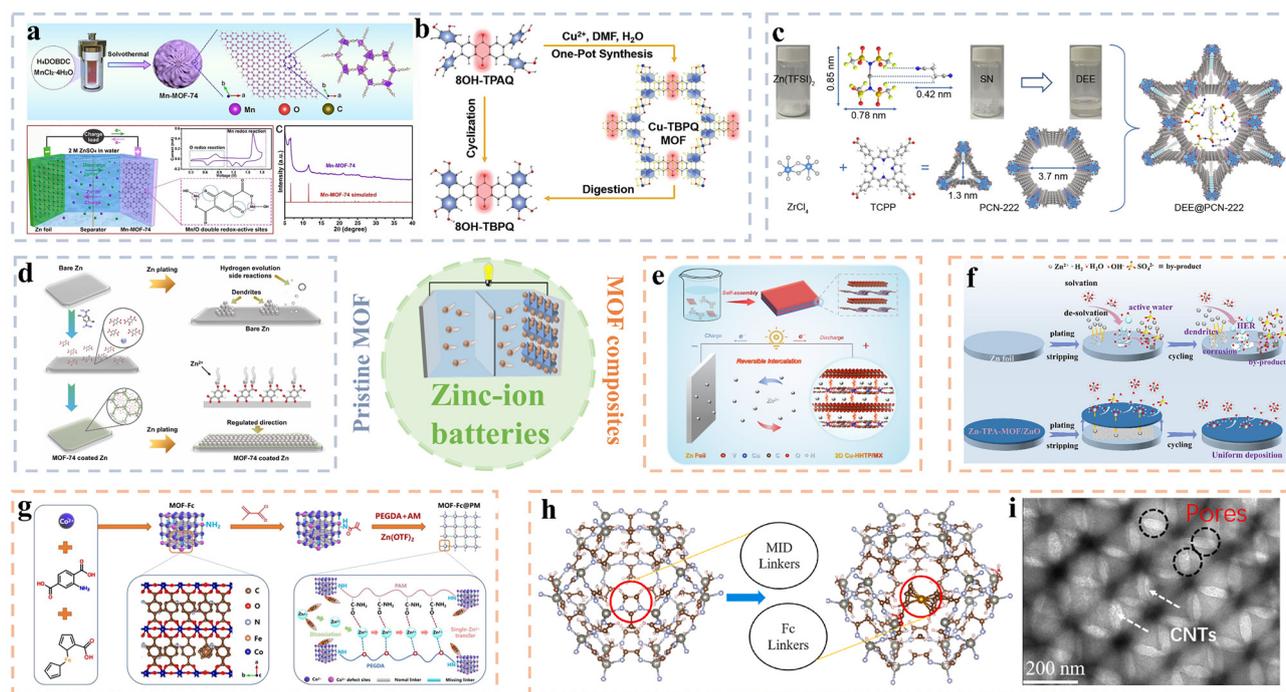
Fig. 10 MOF-based materials for ZIBs. The applications of MOF-based materials for ZIBs. (a) Preparation of Mn-MOF-74.[160] Copyright © 2024, Wiley–VCH. (b) Schematic illustration of the synthesis process of Cu-TBPQ MOF.[161] Copyright © 2024, Wiley–VCH. (c) Preparation process of DEE@PCN-222.[162] Copyright © 2024, Wiley–VCH. (d) Synthesis schematic illustration of MOF-74 coated Zn and Zn deposition processes on MOF-74 coated Zn and bare Zn.[163] Copyright © 2024, Elsevier. (e) The preparation of 2D Cu-HHTP/MX heterostructure and the mechanism for zinc anode.[164] Copyright © 2022, Wiley–VCH. (f) Inhibition of side reactions and dendrites by Zn-TPA-MOF/ZnO protective layer.[165] Copyright © 2023, Elsevier. (g) Fabrication process and the single conducting mechanism for the MOF-Fc@PM electrolyte.[166] Copyright © 2024, American Chemical Society. (h) Modulation of the electronic structure of ZIF-8 by introducing Fc linkers; (i) TEM image of 3DOM Fc-ZIF-8/CNTs.[20] Copyright © 2024, Elsevier.

redox processes involving manganese and oxygen, utilizing double redox-active sites in conjunction with the co-insertion/extraction of Zn^{2+} and H^+ ions. The electrode demonstrates exceptional stability in the context of ZIBs owing to the coordination effects, achieving a high discharge capacity and voltage plateau that culminates in an energy density of 310 Wh kg^{-1}.[160] To address the challenges associated with the poor electrical conductivity inherent to MOF materials, Chen *et al.* proposed an innovative approach by incorporating quinone moieties into a two-dimensional MOF structure.[161] Through a hydrothermal synthesis method, Cu^{2+} was coordinated with an anthraquinone-based multitopic catechol ligand (2,3,6,7-tetrakis (3,4-dihydroxyphenyl) anthracene-9,10-dione (8OH-TPAQ)), resulting in the formation of a graphene-like crystalline material designated as Cu-TBPQ MOF (Fig. 10b). The Cu-TBPQ framework is characterized by abundant porosity, superior electrical conductivity, and multiple redox sites. Its square planar CuO_4 coordination structure, coupled with a high degree of π–d conjugation, ensures excellent stability and restricts the leaching of organic quinone ligands. Furthermore, the dual quinone moieties and $[CuO_4]$ coordination nodes within the structure facilitate significant reversible Zn^{2+} insertion and extraction behaviors, making Cu-TBPQ a promising candidate for zinc-ion battery cathodes.

The design of electrolytes for zinc ion batteries is crucial for enhancing their electrochemical performance. Xu *et al.*

developed stable solid-state electrolytes (SSEs) featuring a Zn^{2+} transport channel by confining a deep eutectic electrolyte (DEE) within a nano-channel of the metal–organic framework (MOF)-PCN-222 (DEE@PCN-222).[162] This confinement increased the number of migration sites for Zn^{2+} and established an ion transport network with PCN-222, facilitating efficient Zn^{2+} transport and ensuring uniform Zn deposition (Fig. 10c). The resulting SSE demonstrated a high ionic conductivity of 3.13×10^{-4} S cm^{-1} and a substantial Zn^{2+} transfer number of 0.74. Furthermore, the specially designed channel structure effectively regulated Zn^{2+} distribution, preventing side reactions and leading to outstanding discharge capacity and cycling stability.

The detachment of metal ions from the cathode contributes to the corrosion of the zinc anode and promotes the growth of dendrites, which significantly undermines the electrochemical performance of zinc ion batteries. Liang *et al.* developed an innovative interfacial modification layer by growing MOF-74 *in situ* on the surface of a zinc anode (Fig. 10d) using a mild acidic solution of 2,5-dihydroxyterephthalic acid (DHTA) in methanol.[163] The incorporation of zincophilic sites and porous structure *via* MOF-74 effectively enhances the surface characteristics of the zinc anode, accelerates the solvation process of zinc ions, facilitates uniform zinc deposition, and inhibits dendrite growth. This enhancement notably improves the corrosion resistance of the zinc anode, resulting in a full cell

with the α-MnO$_2$ cathode that demonstrates exceptional electrochemical stability. Additionally, Yu et al. employed nanoparticles with a pore size of 6.0 Å to protect the anode, taking into account the sizes of zinc ions (4.30 Å) and vanadium ions (8.34 Å) to create a selective ion-permeable layer.[167] This layer ensures a uniform flux of Zn^{2+} ions and directs consistent zinc deposition. Furthermore, the protective layer's influence on vanadium ions effectively reduces the corrosion reaction, resulting in an impressive capacity retention of 86% after 2000 cycles under full cell conditions. This approach serves as a valuable reference for other cathode materials aiming to achieve prolonged cycle stability in zinc ion batteries.

5.2. Composite MOF and functional materials

The inadequate electrochemical performance of ZIBs can be attributed to the stacking of pristine MOF particles, coupled with their poor electrical conductivity and limited chemical stability. A viable solution involves combining pristine MOF materials with highly conductive substrates to construct hybrid materials. For instance, Fu et al. employed CNTs characterized by high surface area, superior conductivity, and chemical stability as a substrate, on which manganese-based MOF (Mn-MOF) was synthesized in situ via solvothermal methods.[40] The resultant Mn-MOF/CNT composite, which demonstrates significant porosity and conductivity, effectively transforms the compact Mn-MOF structure into a conductive network with crosslinked properties. This modification substantially enhanced the overall conductivity and mitigated the discontinuities inherent in the original MOF particles, leading to high discharge capacities and nearly 100% capacity retention when utilized as cathode materials in ZIBs. Similarly, Wong et al. utilized a liquid-phase method to assemble chemically exfoliated 2D MOF material (Cu-HHTP) with modified V$_2$CT$_x$ MXene (MX) to create the Cu-HHTP/MX composite, which embodies an alternating stacked structure (Fig. 10e).[164] The inclusion of MX nanosheets not only augmented the overall conductivity of the composite but also constrained the stacking of Cu-HHTP during repeated charge–discharge cycles. In this configuration, the Cu-HHTP layers serve dual purposes: acting as active storage sites for Zn^{2+} ions while simultaneously providing isolation for the spacer MX nanosheets. The open-plane architecture of the Cu-HHTP/MX heterostructure facilitates the rapid insertion and extraction of Zn^{2+}, resulting in enhanced specific discharge capacity, rate performance, and prolonged cycle stability. To deal with the problems tied to solid-state polymer electrolytes, like the low ionic conductivity and the limited transfer numbers for Zn^{2+} along with issues at the electrolyte-electrode interfaces, Xu and others came up with a poly(ethylene glycol)diacrylate (PEGDA)/polyacrylamide (PAM) copolymer solid electrolyte (Fig. 10f).[166] They used a special missing-linker MOF catalyst in their design. This innovative approach promotes zinc ion (Zn^{2+}) conduction while ensuring robust interfacial contact. Specifically, OTF anions anchored to the unsaturated metal sites of the missing-linker MOF facilitate Zn^{2+} conduction, while the ligand competition for Zn^{2+} ions, engendered by the interaction between PEGDA and PAM chains,

accelerates the transfer of Zn ions. The engineered SPEs exhibit remarkable ionic conductivity and an elevated ionic transfer number, thus fostering uniform deposition of zinc metal and achieving high coulombic efficiency. Chen et al. introduced functionalized Zr–Zn bimetallic UiO-66 as a sacrificial layer on the surface of the Zn anode, where the intrinsic electronegativity of the carboxyl groups enhanced the capture and transport of Zn^{2+} through the anode–electrolyte interface within its channels.[168] Additionally, the introduction of this MOF layer simultaneously suppresses the passivation of the Zn surface, enabling the Zn metal battery to exhibit 4000 h of cycling stability and low overpotential.

To develop a highly reversible zinc anode for ZIBs, Lin et al. designed a hybrid interface protection layer composed of a Zn-terephthalate metal–organic framework (Zn-TPA-MOF) and ZnO (Zn-TPA-MOF/ZnO) (Fig. 10g).[165] This layer stabilizes the surface of pre-oxidized zinc foil, inhibits side reactions, and prevents dendrite growth, thereby enhancing the reversibility of the zinc anode. The strong hydrophobicity and zincophilicity of the Zn-TPA-MOF/ZnO interface facilitate the rapid desolvation of Zn(H$_2$O)$_6^{2+}$ and improve the deposition kinetics of Zn^{2+}. Furthermore, the synergistic properties of this hybrid interface—such as high ionic conductivity, low resistivity, elevated transfer number of Zn^{2+}, and low activation energy—significantly promote the uniform deposition of Zn^{2+}. The Zn-TPA-MOF/ZnO@Zn||Zn-TPA-MOF/ZnO@Zn cell demonstrated remarkable stability over 3020 hours and maintained a high capacity retention across 1000 cycles. In a different approach, Li et al. modified the structure of ZIF-8 using ferrocene formic acid and incorporated highly conductive CNTs to create 3D ordered macroporous structural complexes (3DOM Fc-ZIF-8/CNTs) with a high degree of openness (Fig. 10h and i).[20] This modified structure, enhanced by the Fc linker, exhibits a strong affinity for Zn^{2+}, facilitating uniform nucleation of zinc and suppressing dendrite growth during the plating and stripping processes. The conductive network formed by the introduced CNTs further boosts the conductivity of the modified layer. As a result of this synergistic effect, the Zn@Fc-ZIF-8/CNTs symmetric cell achieved impressive cycling stability—4000 hours at 0.25 mA cm^{-2} and over 1500 hours at 5 mA cm^{-2}. Moreover, the structure designed for full cells integrated with VO$_2$ exhibited high discharge capacity and exceptional cycling stability.

5.3. MOF derivatives carbon-based materials

Manganese-based materials, particularly oxides, serve as two of the primary cathode materials for ZIBs. They offer advantages such as low cost, abundant availability, and environmental friendliness. However, their performance is significantly limited by poor rate performance and capacity decay due to the leaching of manganese ions. In contrast, vanadium-based oxide materials exhibit multiple valence states (V^{2+}, V^{3+}, V^{4+}, V^{5+}) and have open crystal structures that provide high theoretical specific capacity and excellent cycling stability. Nonetheless, their low electronic and ionic conductivity hinders their electrochemical performance. To address the limitations of both manganese and vanadium-based materials, introducing

highly conductive carbon materials like CNTs and rGO into the cathode can effectively enhance conductivity and improve reaction kinetics. MOF materials incorporating Mn/V metal centers along with organic ligands can form a dense carbon layer that encapsulates metal oxide nanoparticles during high-temperature thermal polymerization. This carbon layer not only improves the electrical conductivity of the materials but also maintains the structural stability of the oxides. Furthermore, it specifically helps inhibit the detachment of manganese ions from manganese-based materials. Employing MOF-derived manganese/vanadium-based carbon complexes presents a promising approach for developing cathode materials for ZIBs.

Chen et al. employed Mn-BTC as a precursor for the preparation of MnO/C and Mn_2O_3 through calcination in air and argon environments, respectively.[169] The resultant MnO/C exhibited an abundance of oxygen vacancy defects, which were instrumental in modulating both the electronic properties and microstructural characteristics of the material. These oxygen vacancies not only significantly enhanced the electrical conductivity but also enriched the electrochemical reactive sites, thereby facilitating improved reaction kinetics and overall electrochemical performance. Notably, the MnO/C derived from Mn-MOF as a cathode material for ZIBs demonstrated superior discharge-specific capacity when compared to other manganese-based oxides. However, the electrochemical reaction process is largely constrained by the leaching of Mn^{2+} ions and the limited presence of large, stable channels, specifically concerning the $Mn^{2+} \leftrightarrow Mn^{4+}$ redox process. Liu et al. synthesized layered MOF materials with a hexagonal tunnel structure (L-MOF-HT) utilizing an epitaxial growth strategy based on MOFs, followed by high-temperature calcination.[170] The resulting derivatives, consisting of a MnO@carbon framework (t-MnO@C), maintained the original hexagonal tunneling structure, which, with a diameter of 0.55 nm, facilitated improved ion transport and diffusion within the MnO material. This structural configuration provided an increased number of active sites for Zn^{2+} storage, thereby enhancing the electrochemical redox reaction between Mn^{2+} and Mn^{4+}. The formation of Mn–O–C bonds, induced by the confinement of MnO nanoparticles within a carbon matrix, effectively mitigated the dissolution of Mn^{2+}

ions into the electrolyte. Consequently, the manganese-based oxide composites generated through this methodology demonstrated enhanced discharge-specific capacity and remarkable cycling stability. Cai et al. fabricated nitrogen-doped V_2O_3 (p-NVO@C) microparticles with a porous carbon coating, utilizing vanadium-based zeolite imidazole frameworks (V-ZIFs) as precursors (Fig. 11a).[171] The implementation of nitrogen doping and carbon coating strategies effectively augmented the conductivity of the cathode materials. The bound spaces created by the carbon layer served to limit vanadium dissolution, while the porous architecture retained by the V-ZIFs effectively alleviated the volume expansion induced by Zn^{2+} intercalation and minimized the ionic migration distance. Owing to these multifaceted advantages associated with the MOF-derived vanadium-based oxide materials, p-NVO@C exhibited an exceptional discharge-specific capacity of 501 mAh g^{-1} at a current density of 0.2 A g^{-1}, alongside excellent cycling stability, as evidenced by a capacity retention rate of 95.7% after 2000 cycles at a high current density of 10 A g^{-1}.

Uncontrolled dendrite growth and corrosion-induced instability in zinc metal negative electrodes have significantly impeded the practical application of ZIBs. To tackle the anode challenges, Wang et al. introduced a dendrite-free Zn-3D@600 anode created through high-temperature calcination of ZIF-8. This design features a MOF-derived Zn@C protective layer coated onto a 3D Zn skeleton.[172] The porous carbon skeleton derived from the metal–organic framework (MOF) serves dual purposes: it provides nucleation sites for Zn^{2+} deposition and modulates the ion concentration gradient on the anode surface, effectively suppressing dendrite growth. Furthermore, the 3D porous structure enhances the wettability of the electrolyte while reducing the ion transport distance. Additionally, the skeleton can accommodate minor protrusions resulting from the plating and stripping of Zn during extended cycling, thereby preventing the formation of dead Zn and mitigating capacity degradation and premature cell failure. This innovative structure demonstrates low voltage polarization and long cycle stability in real cells, with no dendrite formation observed even after 1000 cycles. In another approach, Chen et al. utilized UiO-66-NH_2-polysiloxane-derived material as the base material
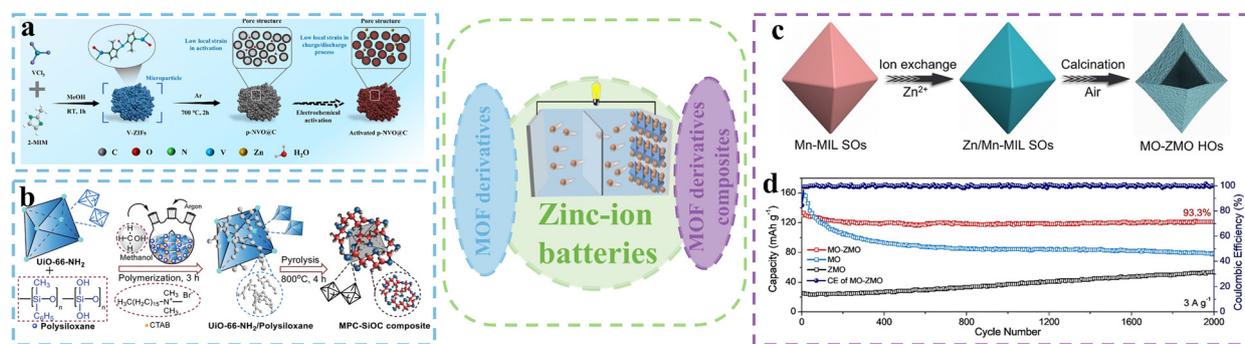

Fig. 11 MOF–based materials for ZIBs. (a) Synthesis and structure of p-NVO@C.[171] Copyright © 2024, Elsevier. (b) Schematic presentations of the synthesis of MPC–SiOC.[173] Copyright © 2024, Wiley–VCH. (c) Schematic illustration of the synthetic process of MO–ZMO Hos; (d) the long cycle performance of at current density of 3 A g^{-1}.[174] Copyright © 2021, Wiley–VCH.

to create a mesoporous carbon-silicon oxycarbide hybrid composite (3DP-MPC-SiOC) using a 3D printing technique (Fig. 11b).[173] This composite forms an interface with zincophilic properties that inhibit dendrite growth. The custom-designed 3D-printed rigid structure generates a uniform electric field on the anode surface, resulting in reduced voltage polarization and promoting long-cycle, dendrite-free growth. The hybrid materials, consisting of carbon structures and SiOC, provide nucleation sites for Zn, encourage uniform deposition of Zn^{2+}, and enhance the ion diffusion rate, facilitating dendrite-free growth while lowering the nucleation barrier. This strategy realized a 198-hour cycle of dendrite-free growth and offers valuable insights for constructing dendrite-free zinc anodes.

5.4. MOF derivative composite with functional materials

Despite the commendable electrochemical performance of manganese/vanadium-based cathode materials synthesized from MOFs, their intrinsic physicochemical properties pose limitations to high-capacity and long-cycle performance. Consequently, the strategic modulation of composition, structure and interfacial properties through constructing complexes derived from MOF derivatives is recognized as an optimal approach to enhance these attributes.

Lou *et al.* developed Mn_2O_3–$ZnMn_2O_4$ (MO–ZMO HOs) heterostructures featuring hollow polyhedral architectures through ion exchange and calcination, utilizing Mn-MIL as the precursor (Fig. 11c and d).[174] These hollow heterostructures possess unique compositions, providing the MO–ZMO HOs with a wealth of active sites, improved electrical conductivity, and exceptional structural stability. Leveraging the distinct advantages of these MOF-derived complexes, they demonstrate high reversible capacity and remarkable energy density when employed as cathode materials for zinc ion batteries. To address the practical challenges posed by the Jahn–Teller effect related to Mn^{2+} dissolution, Chen *et al.* created a co-doped MnO anode material (ZnCo–MnO/C) by incorporating Co and Zn ions, which work synergistically to enhance the electrochemical performance of the MnO cathode.[175] The introduction of Zn ions improves the specific capacity of MnO during the initial activation phase, while the valence state changes of Co ions during cycling not only boost capacity but also significantly mitigate the dissolution of Mn^{2+} during discharge, thereby enhancing structural stability. Furthermore, the doping of heterogeneous metal ions modifies the electronic structure of MnO, resulting in improved electrical conductivity and ion diffusion rates. When combined with a Ti_3C_2@Zn anode to create a full battery, this system demonstrates excellent discharge capacity and cycling performance.

The limited reversibility and slow Zn^{2+} diffusion kinetics of vanadium-based materials lead to inferior multiplicative properties and cycling stability. Li and colleagues introduced a conducting polymer, polyaniline (PANI), as an intercalation molecule into vanadium-MOF-derived hierarchical porous V_2O_5 (PVO).[18] This nanobelt-like PVO possesses a high density of electrochemically active sites and reduces the transport distance for both electrons and ions. The incorporation of PANI

not only broadens the Zn^{2+} diffusion channels but also serves as an interlayer column that enhances the structural stability of the material. Additionally, PANI functions as a conductive polymer, significantly increasing the overall electrical conductivity and diminishing the electrostatic interactions between Zn^{2+} and the PVO host, effectively preventing the collapse of the lamellar structure. Consequently, the PVOs demonstrate remarkable rate performance (375 mAh g^{-1} at 5.0 A g^{-1}) and commendable cycling stability (91.8% capacity retention after 2000 cycles at 8.0 A g^{-1}). The inherent low conductivity and narrow interlayer spacing of V_2O_5 significantly influence the kinetic processes of the electrode. Liu *et al.* employed a "three-in-one" strategy to incorporate Ce ions and PANI into V-MOF-derived porous V_2O_5 (CPVO).[19] The CPVO features a high specific surface area and a nanosheet-like porous structure, providing increased Zn^{2+} diffusion channels and electrochemically active sites, which accelerates the Zn^{2+} migration rate. The combined energy storage mechanism of "interlayer engineering" and "structural deformation confinement," facilitated by the co-embedded Ce ions and PANI, substantially enlarges the interlayer spacing and weakens the electrostatic interactions between the host material and Zn^{2+}. When utilized as cathode materials for zinc-ion batteries, they exhibit outstanding electrochemical properties.

To address the issue of uncontrollable dendrite growth in zinc anodes, Pang *et al.* developed CuZn alloy nanosheets (CuZn@C NSs) with a carbon coating. This was achieved by uniformly growing ZIF-8 on CuO nanosheets and subsequently treating them in a high-temperature reducing atmosphere (H_2/Ar).[176] The presence of Cu–Zn and Zn–N bonds in the CuZn@C NSs serves as zincophilic sites that effectively adsorb Zn^{2+}, facilitating the modulation of deposition behavior and inhibiting dendrite growth. Additionally, the CuZn@C NSs provide a barrier that prevents direct contact between the zinc anode and the electrolyte, significantly reducing the occurrence of side reactions. As a result, these nanosheets demonstrate excellent capacity retention and minimal voltage polarization when utilized in zinc-ion full batteries.

5.5. Summary

Although vanadium- and manganese-based oxides remain among the most promising ZIB cathodes because of their high capacity and favorable redox chemistry, their practical deployment is limited by poor electronic/ionic conductivity, structural degradation (Mn leaching, Jahn–Teller distortions), and incomplete reversibility. Effective cathode strategies combine nanoscale engineering (particle downsizing, hollow/porous morphologies) with conductive integration (conformal carbon, CNT/graphene/MXene coatings, or embedded conductive polymers) and compositional tuning (heteroatom doping, oxygen vacancies, pre-intercalated/pillaring ions). These approaches shorten diffusion paths, accommodate strain, suppress dissolution, and accelerate reaction kinetics—as illustrated by MOF-derived MnO/C and N-doped V_2O_3@C examples that retain framework porosity while limiting metal loss and volume change. On the anode and interfacial side, suppressing dendrites and controlling corrosion

are equally essential. Constructing zincophilic, ion-permeable interfaces (MOF coatings, Zn-TPA-MOF/ZnO layers, selective pore sieves, or MOF-templated 3D carbon hosts) promotes uniform Zn^{2+} flux, lowers nucleation overpotentials, and prevents parasitic reactions. Complementary electrolyte engineering (high-salt, additives, or MOF-confined deep-eutectic electrolytes) further stabilizes deposition and reduces hydrogen evolution.

MOFs are uniquely positioned to address both electrodes simultaneously: they offer tunable pore chemistry and metal-site design for selective Zn^{2+} adsorption, act as templated precursors for conductive, heteroatom-doped carbon shells that lock in metal oxides and form functional interlayers that regulate ion transport. To translate these advantages, future work must couple targeted MOF chemistry (ligand/node selection and pyrolysis control) with electrode architecture—validating designs with *operando* spectroscopy/imaging and full-cell tests at realistic loadings. Only by integrating materials design, interfacial control, and device-level validation can MOF-enabled ZIBs achieve the stability, reversibility, and scalability required for practical applications.

6. Conclusions and outlooks

This review summarizes recent advancements in MOF-based materials for advanced rechargeable batteries, highlighting both the opportunities and challenges associated with harnessing their unique compositional and structural advantages for energy storage and conversion (Fig. 12). We focus on the intrinsic porous structures, abundant active sites, and tunable chemical components of MOFs, examining their roles in ion storage, modulation of metal ion deposition, and facilitation of electrochemical reactions. The electrochemical performance of MOF-based materials across various battery applications is further detailed in Table 1. Despite their promising properties, several critical challenges remain that must be addressed to realize the full potential of MOF-based materials in next-generation high-performance energy storage devices.

(1) Challenges in electrical conductivity and structural stability of pristine MOFs: the limited electrical conductivity and susceptibility to electrolyte corrosion of pristine MOF materials present significant challenges for achieving optimal rate performance and cycling stability in battery systems. While incorporating conductive additives into electrodes is a common strategy to enhance electron transfer at the surface, the intrinsically slow electron transport within pristine MOFs constrains their effectiveness. Efforts to develop conductive MOF variants have improved electron conductivity to some extent, yet significant challenges persist, particularly under high current densities. Moreover, although the high porosity of pristine MOFs facilitates electrolyte permeability, their structural vulnerability in various electrolyte environments and during ion storage severely undermines long-term cycling stability.

To address conductivity limitations, several strategies can be employed: (a) enhancing orbital overlap between metal active centers and organic ligands to promote charge transport and improve conductivity; (b) strengthening non-covalent interactions between electrochemically active fragments within the MOF framework to establish efficient electron pathways; (c) introducing guest charge carriers through small-molecule modifications or heterogeneous metal ion incorporation to improve conductivity *via* interactions with the host framework; (d) creating intentional defects within the MOF structure to generate local node deficiencies, thereby altering the electronic environment to facilitate electron transport.

Enhancing the structural stability of MOFs in batteries is a systematic endeavor that typically requires the coordinated application of multiple strategies. The following approaches
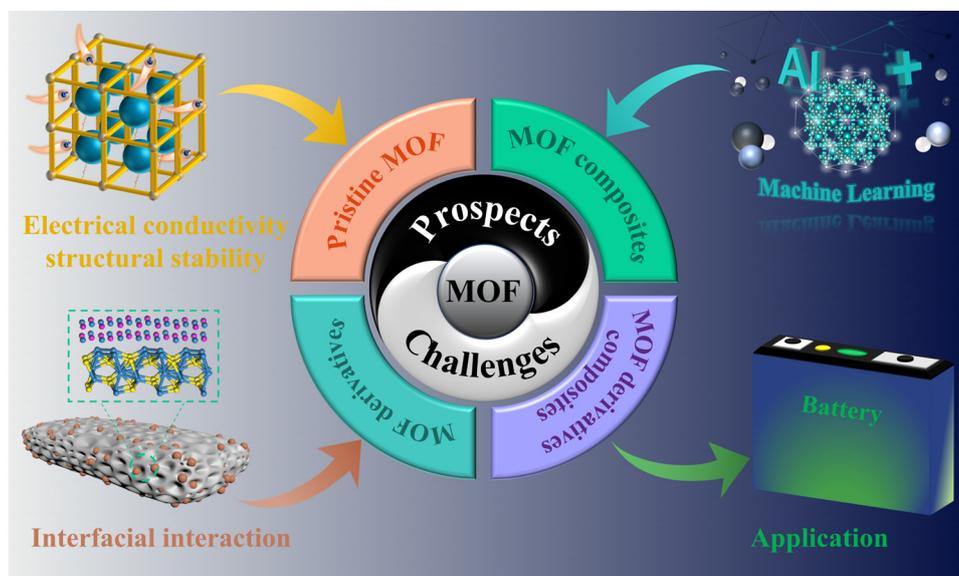

Fig. 12 Prospects and challenges of MOF–based materials for batteries. Including structural stability and conductivity enhancement, data-driven development, interfacial interactions, and applications.

Table 1 Summary of MOF-based materials for energy storage and conversion applications

MOF	Forms of utilization	Application	Rate capacity DSC[a]/CD[b]	Cycle stability DSC/CD/CN[c]	Ref.
Fe-TABQ	Fe-TABQ	LIB anode	$207.1/1$ A g^{-1}	$225/0.2$ A g^{-1}/200	56
CoBPDCA	CoBPDCA	LIB anode	$1112.9/0.05$C	$166.3/10$C/2500	59
Fe-TTTP	Fe-TTTP	LIB anode	$95/10$ A g^{-1}	$310 \pm 20/5000/2$ A g^{-1}	60
Al-MOF	Al-MOF@RGO	LIB anode	—	$468.5/1.0$ A g^{-1}/1000	65
ZIF-67	Co$_3$O$_4$@CNTs	LIB anode	$581/5$ A g^{-1}	$1037.6/1$ A g^{-1}/200	75
CoSn-MOF	CoSn@NC	LIB anode	$229.5/5$ A g^{-1}	$509.3/0.5$ A g^{-1}/500	76
ZIF-8	ZnS nanodots/Ti$_3$C$_2$T$_x$	LIB anode	$252.5/2$ A g^{-1}	$463/0.5$ A g^{-1}/1000	97
Ni(BDC)	Ni(BDC-NH$_2$)/rGO	LIB anode	—	$575.3/1$ A g^{-1}/1000	66
ZIF-8	NPC	LIB anode	$767/2$ A g^{-1}	$738/2$ A g^{-1}/1000	73
ZIF-67	H-Co$_3$O$_4$@MCNBs	LIB anode	$658/2$ A g^{-1}	$1120/0.2$ A g^{-1}/100	77
HKUST-1	LCuTO@HKUST	LIB anode	$132.6/5.0$ A g^{-1}	$160.3/0.5$ A g^{-1}/500	80
Bi-MOF	Bi@CF	LIB anode	$151/5$ A g^{-1}	$306/1.0$ A g^{-1}/900	85
Fe-MOF	Fe$_2$O$_3$@C@N-Ti$_3$C$_2$T$_x$	LIB anode	$226/10$ A g^{-1}	$314/5$ A g^{-1}/2800	98
ZIF-8@ZIF-67	ZnSe@CoSe@CN	LIB anode	$650.8/5$ A g^{-1}	$600/5$ A g^{-1}/1000	101
HE-PBA	HE-PBA	SIB cathode	$62/1$ A g^{-1}	$68/0.5$ A g^{-1}/3000	57
Na$_x$FeFe(CN)$_6$	Na$_x$FeFe(CN)$_6$@rGO	SIB cathode	$96.8/9$ A g^{-1}	$80/1.0$ A g^{-1}/1000	70
NiPBA	IP-PBA@3DUC	SIB cathode	$56/0.4$ A g^{-1}	$47.3/50$ m A g^{-1}/900	69
Co-HAB	Co-HAB	SIB anode	$214/2$ A g^{-1}	$185/4$ A g^{-1}/150	62
ZIF-67	CoS/C HC	SIB anode	$600/5$ A g^{-1}	$600/2.0$ A g^{-1}/500	49
ZIF-67	CoS$_2$@CNTs	SIB anode	$406.5/5$ A g^{-1}	$509/1$ A g^{-1}/200	75
dia-Co (MeIm)$_2$	CoPSe/NC	SIB anode	$292/5$ A g^{-1}	$223/5$ A g^{-1}/3000	102
ZIF-8	NPC	SIB anode	$326.0/3$ A g^{-1}	$238.5/5$ A g^{-1}/1000	73
Co (Salen)	CoS@HDC	SIB anode	$300/1$ A g^{-1}	$330/0.5$ A g^{-1}/1000	78
Pb-MOF	Pb@C	SIB anode	$124.1/5$ A g^{-1}	$334.2/2$ A g^{-1}/6000	89
Fe-MOF	Fe$_2$O$_3$@C@N-Ti$_3$C$_2$T$_x$	SIB anode	$135/5$ A g^{-1}	$209/2$ A g^{-1}/3000	98
ZIF-8@ZIF-67	ZnSe@CoSe@CN	SIB anode	$331/5$ A g^{-1}	$397.3/5$ A g^{-1}/1000	101
In-MOF	In$_2$Se$_3$@C/rGO	SIB anode	$322/5$ A g^{-1}	$393/1$ A g^{-1}/500	104
HAN-Cu-MOF	HAN-Cu-MOF	PIB anode	$161/2$ A g^{-1}	$202.4/1$ A g^{-1}/500	58
Cu-HBB-MOF	Cu-HBB-MOF	PIB anode	$128/10$ A g^{-1}	$103.6/5$ A g^{-1}/2500	63
K-BPDC	NiSA@K-BPDC	PIB anode	$114/2$ A g^{-1}	$146/1$ A g^{-1}/4000	71
dia-Co (MeIm)$_2$	CoPSe/NC	PIB anode	$218/5$ A g^{-1}	$203/5$ A g^{-1}/2000	102
Ni–Co-PBA	Ni–Co–S@rGO	PIB anode	$303/10$ A g^{-1}	$348/10$ A g^{-1}/2000	103
ZIF-8	CNT@ZIF-8	PIB anode	$98/20$C	$88/5$C/1000	72
Sn-MOF	Sn$_3$(PO$_4$)$_2$@PC	PIB anode	$154/5.0$ A g^{-1}	$144/5$ A g^{-1}/10 000	83
Co-MOF	Co$_9$S$_8$@NPC	PIB anode	$194/3.2$ A g^{-1}	$223/1$ A g^{-1}/1000	84
Zn-MOF-74	P@ZCRods	PIB anode	$187.5/5$ A g^{-1}	$150.7/2.5$ A g^{-1}/400	94
Zr-NiS$_4$	Zr-NiS$_4$/S	LSB cathode	$800/3$C	$700/2$C/1200	113
CoNiMOF	S@CoNiMOF	LSB cathode	$535/2$C	$690/0.2$C/400	114
UiO-66-V	CNT@UiO-66-V-S	LSB cathode	$747.7/3$C	$609/1$C/1000	118
HKUST-1	PHK/S	LSB cathode	$630/5$C	$679/5$C/1500	119
CoZn-MOF	S/CoZn-Se@N-MX	LSB cathode	$844/3$C	$361/2$C/2000	52
CoZn-MOF	3d-omsh/ZnS,Co–N–C/S	LSB cathode	$670/5$C	$700/16$C/1000	156
Ni-MOF	S/Ni@PC	LSB cathode	$1014.6/2$C	$417.4/1$C/500	135
MOF UiO-66-NH$_2$	CoS/HNC–S	LSB cathode	$800/1$C	$455/1$C/800	144
CuZn-MOF	Cu SA/NOC/S	LSB cathode	$483/5$ A g^{-1}	$601/1$ A g^{-1}/1000	152
ZIF-8	S@HZIF/CNT	LSB cathode	$696/3$C	$624.6/0.5$C/500	153
Zn–Co MOF	ZnSe-CoSe-HNC/S	LSB cathode	$469.2/5$C	$522/1$C/1000	141
ZIF-8@ZIF-67	CoSe$_2$/Co$_3$O$_4$@NC-CNT/S	LSB cathode	$688/5$C	$602/2$C/500	155
MIP-202	MIP-202@2320	LSB separator	$490/3$C	$614/0.5$C/600	117
aFeNi-MOF	aFeNi-MOF-PP	LSB separator	$728.6/3$C	$538.2/1$C/500	123
Cu-MOF	Cu-MOF-GA	LSB separator	$981.2/3$C	$655.0/0.5$C/400	125
UiO-66	UiO-66/ACNT	LSB separator	$712.1/3$C	$428/1$C/1000	120
PCN-222(Cu)	PCN-222(Cu)-NS	LSB separator	$718.3/3$C	$723.3/1$C/500	148
MOF-801(Zr)	MOF-801(Zr)/C/PVDF-HFP	LSB interlayer	$798/0.2$C	$880/0.1$C/50	128
CoZn-ZIFs	S@Co, N-MPC	SSB cathode	$835.01/3$C	$1134.63/0.2$C/100	136
ZIF-8@ZIF-67	S@HPC/Mo$_2$C	SSB cathode	$483/10$ A g^{-1}	$503/5$ A g^{-1}/800	138
Zn-MOF	MOF-C/S/PDAc	SSB cathode	$201/5.0$ A g^{-1}	$270/1$ A g^{-1}/1000	140
ZIF-8	Y SAs/NC	SSB full cell	$516/10$ A g^{-1}	$510/5$ A g^{-1}/1000	139
ZIF-8	W$_{SA}$–W$_2$C@NC/S	PSB cathode	$697/1$C	—	142
ZIF-67	S–N–Co$_s$–C	PSB cathode	$415/0.4$ A g^{-1}	$355.3/0.2$ A g^{-1}/150	137
MIL-100(V)	MIL-100(V)	ZIB cathode	$277/1$ A g^{-1}	$103/1$ A g^{-1}/3500	159
Mn-MOF-74	Mn-MOF-74	ZIB cathode	$139/0.4$ A g^{-1}	$86.5/0.5$ A g^{-1}/500	160
Cu-TBPQ	Cu-TBPQ	ZIB cathode	$149.6/1$ A g^{-1}	$120.3/2$ A g^{-1}/300	161
Cu-HHTP	Cu-HHTP/MX	ZIB cathode	$170.6/4$ A g^{-1}	$166.9/4$ A g^{-1}/1000	164
L-MOF-HT	t-MnO@C	ZIB cathode	$130/5$ A g^{-1}	$132/5$ A g^{-1}/20 000	170
V-ZIFs	p-NVO@C	ZIB cathode	$257/10$ A g^{-1}	$200/10$ A g^{-1}/2000	171
Zn/Mn-MIL SOs	Mn$_2$O$_3$–ZnMn$_2$O$_4$- HOs	ZIB cathode	$120.2/5$ A g^{-1}	$120/3$ A g^{-1}/2000	174
Mn-MOF	Mn-MOF/CNT	ZIB cathode	$73.5/0.5$ A g^{-1}	$40/1$ A g^{-1}/900	40
ZnCoMn-BTC	ZnCo-MnO/C	ZIB cathode	$62.6/3$ A g^{-1}	$120/2$ A g^{-1}/2000	175
V-MOF	PVO	ZIB cathode	$375/5.0$ A g^{-1}	$268/8$ A g^{-1}/2000	18

Table 1 (continued)

MOF	Forms of utilization	Application	Rate capacity DSC^a/CD^b	Cycle stability DSC/CD/CN^c	Ref.
(MOF)-PCN-222	DEE@PCN-222	ZIB electrolytes	140/5C	240/1C/517	162
MOF-Fc	MOF-Fc@PM	ZIB electrolytes	89.3/5 A g^{-1}	123.9/1 A g^{-1}/2000	166
MOF-74	MOF-74	ZIB anode	208/0.2 A g^{-1}	161/0.2 A g^{-1}/1000	163
MOF-801	MOF-801	ZIB anode	146/5 A g^{-1}	115/5 A g^{-1}/2000	167
Zn-TPA-MOF	Zn-TPA-MOF/ZnO	ZIB anode	89/5 A g^{-1}	106.6/5 A g^{-1}/1000	165
ZIF-8	3DOM Fc-ZIF-8/CNTs	ZIB anode	232/3C	65/1C/500	20
ZIF-8	CuZn@C NSs	ZIB anode	118.8/10 A g^{-1}	105.4/5 A g^{-1}/1000	176

^{a} DSC: discharge specific capacity. ^{b} CD: current density. ^{c} CN: cycle numbers.

may serve as references: (a) Core Design: Design stable MOFs (e.g., Zr-MOF) at the molecular level featuring metal nodes with high connectivity and rigid conjugated ligands. (b) External protection: apply "armor" through ALD coating or carbon material composites to physically isolate the MOF from direct electrolyte contact, preventing solvent co-intercalation and side reactions. (c) Environment optimization: employ electrolyte additives that form stable SEI films alongside robust binders.

(2) Advantages and challenges of MOF-derived carbon materials: the rich pore structure, high specific surface area, abundant active sites, and enhanced electrical conductivity of MOF-derived carbon materials—obtained from the original MOFs—offer significant advantages for ion storage and catalytic conversion. However, microstructural damage caused by particle aggregation and structural collapse during the high-temperature calcination of pristine MOFs can lead to poor electrochemical performance over prolonged cycling. For electrode materials, the favorable properties of high porosity and large surface area facilitate electrolyte penetration, ion transport, and accessibility of active sites. Yet, these same attributes can also result in low coulombic efficiency and reduced bulk density, which hinder the development of high-performance energy storage devices.

To mitigate particle stacking and structural issues, several strategies can be employed: (a) incorporating matrix materials such as CNTs, rGO, or MXenes to spatially separate MOF particles; (b) chemically modifying the surface of original MOF particles—through functional group alteration or surface coatings—to prevent stacking during calcination; (c) optimizing high-temperature treatment conditions, including time, atmosphere, and temperature, to control calcination kinetics and prevent uncontrolled particle growth during carbonization.

Additionally, precise regulation of pore size and specific surface area can significantly enhance electrochemical performance. However, systematic manipulation of pore architecture in MOF derivatives remains relatively underexplored in energy storage and conversion applications. Further research is needed to establish optimized preparation and calcination parameters that maximize the properties and performance of MOF-derived carbon materials.

(3) Understanding interactions in pristine MOFs and their derivative composites: the interactions between the constituent materials in pristine MOFs and their derivative composites remain inadequately understood. Electronic interactions between MOFs and functionalized compounds are critical for enhancing ion storage capacity and accelerating catalytic reaction kinetics. Currently, most MOF-based material complexes reported in the literature are primarily characterized by their electrochemical performance, leaving the underlying mechanisms responsible for the observed synergistic enhancements largely unexplored.

There is a pressing need for comprehensive studies aimed at elucidating the roles of individual components in MOF-based complex materials. Such investigations can deepen our understanding of ion storage and reaction mechanisms at each stage of the electrochemical process, ultimately guiding the design of more efficient energy storage devices. Key areas for exploration include: (a) the intrinsic mechanisms by which small molecule functional groups improve the electrochemical performance of MOFs; (b) localized electronic interactions generated by multi-component heterojunctions that enhance electronic conductivity and catalytic activity; (c) development of multi-reactive active sites that facilitate electrochemical reactions. Furthermore, rigorous analysis of the structure–function relationship, particularly regarding enhancements in electrochemical performance, is essential to fully realize the potential of MOF-based material complexes for high-efficiency energy storage.

(4) Big data and artificial intelligence for MOF materials design: the emergence of big data and artificial intelligence (AI) has established a new paradigm for data-driven materials research and development, offering the potential to enhance research efficiency and accelerate industrial applications significantly. Tens of thousands of MOF materials with diverse compositions and structural features currently exist. However, most research focuses on selecting individual materials and applying composite strategies to evaluate their electrochemical performance. In contrast, integrating big data analytics and AI for high-throughput screening and predictive design of MOF materials can markedly expedite the development process, enabling more targeted exploration of promising candidates for energy storage applications.

(5) Cost, yield, and scalability considerations for MOF-based materials: practical application of MOF-based materials in next-generation high-efficiency batteries requires addressing issues of high cost and low yield. Low material yields, long preparation times, high costs, and complex synthetic processes often limit current laboratory-scale research. Streamlined, efficient, and cost-effective preparation methods are essential to overcome these barriers. Additionally, significant material loss during high-temperature pyrolysis of MOF derivatives further complicates scalability. While MOF-based materials demonstrate

impressive electrochemical performance at the laboratory scale, comprehensive cost–benefit analyses are necessary for large-scale implementation. Beyond cost considerations, the strong overall performance of MOFs positions them as promising candidates for high-performance energy storage. Industrial adoption will depend on reducing costs—particularly for organic ligands—and simplifying preparation processes without compromising material performance.

In summary, recent advancements in the development and design of MOF-based materials have significantly advanced energy storage and conversion technologies. Nevertheless, constructing MOF-based nanostructured materials with high ion storage capacity and catalytic efficiency still requires further investigation. New strategies are essential to enhance both the stability and electrical conductivity of these materials. Addressing challenges such as particle aggregation and structural collapse in MOF derivatives remains critical for long-term performance.

A deeper understanding of the interaction mechanisms among multiple components in MOF-based materials is necessary to achieve synergistic improvements in electrochemical performance. Additionally, the integration of big data and artificial intelligence offers powerful tools for data-driven screening and predictive design, accelerating the development of high-performance MOF-based materials. Cost-effective, high-efficiency preparation methods are also crucial for enabling large-scale applications. Despite these challenges, the future of MOF-based materials in electrochemical energy storage and conversion is promising, with opportunities driven by structural optimization, compositional tuning, and comprehensive theoretical and mechanistic studies.

Author contributions

Conceptualization, X. W., L. T., and W. Y.; writing – original draft, X. W., Z. D., and H, T.; writing – review & editing, X. W., L. T., and W. Y.; funding acquisition, L. T.; supervision, L. T.; all authors were involved in the discussion and review of the review.

Conflicts of interest

The authors declare no conflicts of interest.

Data availability

No primary research results, software or code has been included and no new data were generated or analyzed as part of this review.

Acknowledgements

References

1 T. Liu, Y. Yang, S. Cao, R. Xiang, L. Zhang and J. Yu, *Adv. Mater.*, 2023, **35**, 2207752.

2 S. Chu and A. Majumdar, *Nature*, 2012, **488**, 294–303.

3 G. Goel, M. Sharma and S. K. Tripathi, *J. Energy Storage*, 2025, **126**, 116995.

4 Y. Ma, L. Zhang, Z. Yan, B. Cheng, J. Yu and T. Liu, *Adv. Energy Mater.*, 2022, **12**, 2103820.

5 Y. Peng, J. Xu, J. Xu, J. Ma, Y. Bai, S. Cao, S. Zhang and H. Pang, *Adv. Colloid Interface Sci.*, 2022, **307**, 102732.

6 Z. Ye, Y. Jiang, L. Li, F. Wu and R. Chen, *Nano-Micro Lett.*, 2021, **13**, 203.

7 R. Fu, L. Wang, K. Wang, C. Li, M. Ouyang, C. Zhang, H. Wu and Q. Zhang, *Coord. Chem. Rev.*, 2025, **541**, 216832.

8 O. M. Yaghi and H. Li, *J. Am. Chem. Soc.*, 1995, **117**, 10401–10402.

9 R. Sakamoto, N. Fukui, H. Maeda, R. Toyoda, S. Takaishi, T. Tanabe, J. Komeda, P. Amo-Ochoa, F. Zamora and H. Nishihara, *Coord. Chem. Rev.*, 2022, **472**, 214787.

10 X. Wang, Q. Wei, H. Li, J. Sun, H. Li, Y. He and Z. Liu, *J. Mater. Chem. A*, 2022, **10**, 7517–7556.

11 X. Xiao, L. Zou, H. Pang and Q. Xu, *Chem. Soc. Rev.*, 2020, **49**, 301–331.

12 X. X. Liu, L. Pan, H. Zhang, C. Liu, M. Cao, M. Gao, Y. Zhang, Z. Xu, Y. Wang and Z. Sun, *Nano-Micro Lett.*, 2025, **17**, 249.

13 I. Shahid, N. H. Solangi, R. Andavar, F. Ullah, Y. Sun, U. A. Kolachi, J. Xie, X. Li and J. Pan, *Chem. Eng. J.*, 2025, **514**, 163273.

14 X. Tang, C. Liu, H. Wang, L. Lv, W. Sun and Y. Wang, *Coord. Chem. Rev.*, 2023, **494**, 215361.

15 W. Wang, D. Chen, F. Li, X. Xiao and Q. Xu, *Chem*, 2024, **10**, 86–133.

16 H. Jiang, X. Liu, Y. Wu, Y. Shu, X. Gong, F. Ke and H. Deng, *Angew. Chem., Int. Ed.*, 2018, **57**, 3916–3921.

17 Y. Wang, F. Cheng, J. Ji, C. Cai and Y. Fu, *Carbon Energy*, 2024, **6**, e520.

18 Y. Zhang, Z. Li, M. Liu and J. Liu, *Chem. Eng. J.*, 2023, **463**, 142425.

19 Y. Zhang, Z. Li, B. Zhao, Z. Wang and J. Liu, *J. Mater. Chem. A*, 2024, **12**, 1725–1735.

20 Y. Xu, X. Li, X. Wang, Q. Weng and W. Sun, *J. Power Sources*, 2024, **624**, 235525.

21 W. Zhu, G. Wang, S. Zhou, Y. Min, C. Yang and J. Huang, *New J. Chem.*, 2024, **48**, 17961–17968.

22 R. Zhang, C. Lv, S. Bao, J. Gao, Y. Xie, F. Zheng, X. Liu, Y. Wen and B. Xu, *J. Colloid Interface Sci.*, 2022, **628**, 154–165.

23 J. B. Lim, J. H. Na, H. J. Kim, J. K. Kim, Y. Yoo and S.-K. Park, *J. Alloys Compd.*, 2024, **1002**, 175507.

24 G. Dey, S. Saifi, H. Sharma, M. Kumar and A. Aijaz, *ACS Appl. Nano Mater.*, 2023, **6**, 8192–8201.

25 Z. Zhang, L. Kong, S. Liu, G. Li and X. Gao, *Adv. Energy Mater.*, 2017, **7**, 1602543.

26 H. Wang, L. Chen, H. Pang, S. Kaskel and Q. Xu, *Chem. Soc. Rev.*, 2020, **49**, 1414–1448.

27 X. Zhang, A. Chen, M. Zhong, Z. Zhang, X. Zhang, Z. Zhou and X.-H. Bu, *Electrochem. Energy Rev.*, 2018, **2**, 29–104.

28 Z. Li, J. Wang, H. Yuan, Y. Yu and Y. Tan, *Adv. Funct. Mater.*, 2024, **34**, 2405890.

29 L. Tian, P. Huang, J. Lv, Y. Zhang, L. Zhao, L. Liu, P. Wang, Y. Wu, Q. Shi and F. Shi, *J. Solid State Chem.*, 2024, **335**, 124717.

30 B. Li, Z. Ju, M. Zhou, K. Su and D. Yuan, *Angew. Chem., Int. Ed.*, 2019, **58**, 7687–7691.

31 N. Kitchamsetti and J. S. Cho, *J. Energy Storage*, 2024, **80**, 110293.

32 T. De Villenoisy, X. Zheng, V. Wong, S. S. Mofarah, H. Arandiyan, Y. Yamauchi, P. Koshy and C. C. Sorrell, *Adv. Mater.*, 2023, **35**, 2210166.

33 M. Sadakiyo, T. Yamada and H. Kitagawa, *J. Am. Chem. Soc.*, 2009, **131**, 9906–9907.

34 M. G. Campbell, D. Sheberla, S. F. Liu, T. M. Swager and M. Dincă, *Angew. Chem., Int. Ed.*, 2015, **54**, 4349–4352.

35 X. Huang, P. Sheng, Z. Tu, F. Zhang, J. Wang, H. Geng, Y. Zou, C. Di, Y. Yi, Y. Sun, W. Xu and D. Zhu, *Nat. Commun.*, 2015, **6**, 7408.

36 H. B. Son, S. Cho, K. Baek, J. Jung, S. Nam, D. Han, S. J. Kang, H. R. Moon and S. Park, *Adv. Funct. Mater.*, 2023, **33**, 2302563.

37 Z. Li, Y. Sun, X. Wu, H. Yuan, Y. Yu and Y. Tan, *ACS Energy Lett.*, 2022, **7**, 4190–4197.

38 F. Lan, H. Zhao, Y. Jiang, C. Jin, G. Zhao and L. Li, *J. Mater. Chem. A*, 2025, **13**, 7357–7370.

39 J. Meng, X. Liu, C. Niu, Q. Pang, J. Li, F. Liu, Z. Liu and L. Mai, *Chem. Soc. Rev.*, 2020, **49**, 3142–3186.

40 J. Zhang, Y. Liu, T. Wang, N. Fu and Z. Yang, *J. Energy Storage*, 2024, **76**, 109873.

41 H. Zhang, W. Zhao, M. Zou, Y. Wang, Y. Chen, L. Xu, H. Wu and A. Cao, *Adv. Energy Mater.*, 2018, **8**, 1800013.

42 C. Gao, P. Wang, Z. Wang, S. K. Kær, Y. Zhang and Y. Yue, *Nano Energy*, 2019, **65**, 104032.

43 C. Gao, Z. Jiang, P. Wang, L. R. Jensen, Y. Zhang and Y. Yue, *Nano Energy*, 2020, **74**, 104868.

44 A. Radwan, H. Jin, D. He and S. Mu, *Nano-Micro Lett.*, 2021, **13**, 132.

45 X. Wang, B. Zhu, D. Xu, Z. Gao, Y. Yao, T. Liu, J. Yu and L. Zhang, *ACS Appl. Mater. Interfaces*, 2023, **15**, 26882–26892.

46 M. Zhong, L. Kong, N. Li, Y. Liu, J. Zhu and X. Bu, *Coord. Chem. Rev.*, 2019, **388**, 172–201.

47 X. Cao, C. Tan, M. Sindoro and H. Zhang, *Chem. Soc. Rev.*, 2017, **46**, 2660–2677.

48 L. Zhang, B. Zhu, D. Xu, Z. Qian, P. Xie, T. Liu and J. Yu, *J. Mater. Sci. Technol.*, 2024, **172**, 185–195.

49 Y. Yang, Y. Ma, X. Wang, Z. Gao, J. Yu and T. Liu, *Chem. Eng. J.*, 2023, **455**, 140610.

50 Y. Hu, H. Huang, D. Yu, X. Wang, L. Li, H. Hu, X. Zhu, S. Peng and L. Wang, *Nano-Micro Lett.*, 2021, **13**, 159.

51 C. Song, G. Li, Y. Yang, X. Hong, S. Huang, Q. Zheng, L. Si, M. Zhang and Y. Cai, *Chem. Eng. J.*, 2020, **381**, 122701.

52 Z. Ye, Y. Jiang, L. Li, F. Wu and R. Chen, *Adv. Mater.*, 2021, **33**, 2101204.

53 H. Dai, Z. Long, Z. Li, Z. Yan, Q. Wang, K. Wang, Q. Wei and H. Qiao, *J. Alloys Compd.*, 2024, **1007**, 176489.

54 C. An and T. Liu, *Acta Phys. -Chim. Sin.*, 2025, **41**, 100101.

55 Q. Li, P. Li, Z. Liu, J. Zhang, H. Zhang, W. Yu and X. Hu, *Acta Phys. -Chim. Sin.*, 2024, **40**, 2311030.

56 J. Geng, Y. Ni, Z. Zhu, Q. Wu, S. Gao, W. Hua, S. Indris, J. Chen and F. Li, *J. Am. Chem. Soc.*, 2023, **145**, 1564–1571.

57 Y. Ma, Y. Ma, S. L. Dreyer, Q. Wang, K. Wang, D. Goonetilleke, A. Omar, D. Mikhailova, H. Hahn, B. Breitung and T. Brezesinski, *Adv. Mater.*, 2021, **33**, 2101342.

58 M. Yang, X. Zeng, M. Xie, Y. Wang, J. Xiao, R. Chen, Z. Yi, Y. Huang, D. Bin and D. Li, *J. Am. Chem. Soc.*, 2024, **146**, 6753–6762.

59 L. Su, J. Chen, J. Zhou, J. Liu, Z. Hu, S. Li, X. Hu, L. L. Xu and L. Zhang, *Adv. Energy Mater.*, 2024, **14**, 2402489.

60 C. Li, C. Zhang, K. Wang, F. Yu, J. Xie and Q. Zhang, *Chem. Eng. J.*, 2022, **431**, 133234.

61 T. Yuan, Y. Chen, X. Gao, R. Xu, Z. Zhang, X. Chen and L. Cui, *Small Methods*, 2024, **8**, 2301372.

62 J. Park, M. Lee, D. Feng, Z. Huang, A. C. Hinckley, A. Yakovenko, X. Zou, Y. Cui and Z. Bao, *J. Am. Chem. Soc.*, 2018, **140**, 10315–10323.

63 X. Su, L. Cheng, X. Yan, H. Zhang, T. Wang, H.-G. Wang and L. Chen, *J. Am. Chem. Soc.*, 2025, **147**, 18338–18348.

64 Q. Deng, R. Wang, Y. Wang, Z. Yang, B. Gou, J. Li, Y. Yan and R. Yang, *J. Colloid Interface Sci.*, 2022, **628**, 556–565.

65 K. Wang, J. Chen, F. Hou, H. Wang, Y. Zhang, X. Zhong, Y. Song, Y. Zhang, Z. Zhang, H. Liu, J. Liang and H. Wang, *Chem. Eng. J.*, 2023, **455**, 140561.

66 R. Shah, S. Ali, S. Ali, P. Xia, F. Raziq, Adnan, F. Mabood, S. Shah, A. Zada, P. M. Ismail, A. Hayat, A. U. Rehman, X. Wu, H. Xiao, X. Zu, S. Li and L. Qiao, *J. Alloys Compd.*, 2023, **936**, 168183.

67 J. Zhu, X. Liu, X. Zeng, H. Zhu, S. Jia, Y. Qiao, L. Ren, J. Long, J. Lan, Y. Yu and X. Yang, *J. Colloid Interface Sci.*, 2025, **697**, 137993.

68 J.-E. Zhou, Y. Li, X. Lin and J. Ye, *Nano-Micro Lett.*, 2024, **17**, 9.

69 T. Yuan, X. Gao, S. Kang and L. Cui, *Chem. Eng. Sci.*, 2025, **301**, 120669.

70 Y. Tang, L. Wang, J. Hu, M. Chen, M. Zhou, K. Wang and K. Jiang, *Adv. Energy Mater.*, 2024, **14**, 2303015.

71 Y. Li, A. Zhu, G. Peng, J. He, D. Jia, J. Qiu and X. He, *Adv. Funct. Mater.*, 2024, **34**, 2410212.

72 Y. Chen, Z. Liu, Y. Lu, X. Gao, J. Zhou, X. Wang, Q. Gu and W. Luo, *J. Power Sources*, 2024, **613**, 234909.

73 A. Cheng, G. Yu, J. Pu, Z. Gong, J. Liu, S. Wang and J. Mao, *Energy Fuels*, 2024, **38**, 16957–16965.

74 X. Han, Y. Cao, Y.-Y. Liu, C. Li, H. Geng, H. Gu, P. Braunstein and J. Lang, *Adv. Mater.*, 2024, **36**, 2407274.

75 Z. A. Li, S. G. Wang, P. P. Chen, J. T. Lei, Y. L. Hou, J. Z. Chen and D. L. Zhao, *ACS Appl. Mater. Interfaces*, 2024, **16**, 19730–19741.

76 Y. Duan, A. Jiao, Z. Li, S. Zhang, T. Su and Z. Fu, *J. Power Sources*, 2024, **617**, 235146.

77 Y. Huang, Y. Fang, X. F. Lu, D. Luan and X. W. Lou, *Angew. Chem., Int. Ed.*, 2020, **59**, 19914–19918.

78 C. Liu, Q. Lu, M. V. Gorbunov, A. Omar, I. G. Gonzalez Martinez, P. Zhao, M. Hantusch, A. Dimas Chandra Permana, H. He, N. Gaponik and D. Mikhailova, *J. Energy Chem.*, 2023, **79**, 373–381.

79 K. Schlichte, T. Kratzke and S. Kaskel, *Microporous Mesoporous Mater.*, 2004, **73**, 81–88.

80 H. Tang, Y. Wang, X. Liu, T. Tian, Q. Weng, X. Liu and T. Liu, *J. Electroanal. Chem.*, 2024, **968**, 118507.

81 J. Ren, B. Xing, W. Luo, B. Luo, X. Wu, X. Yan, W. Feng, F. Wang, C. Cheng and L. Mai, *Nano Res.*, 2024, **17**, 5138–5147.

82 D. Yu, Q. Song, J. Cui, H. Zheng, Y. Zhang, J. Liu, J. Lv, T. Xu and Y. Wu, *J. Mater. Chem. A*, 2021, **9**, 26181–26188.

83 H. Jiang, S. Zhang, L. Yan, Y. Xing, Z. Zhang, Q. Zheng, J. Shen, X. Zhao and L. Wang, *Adv. Sci.*, 2023, **10**, 2206587.

84 Y. Ma, M. Wu, L. Li, Z. Li, X. Zhao, R. Lian and W. Zhang, *Appl. Surf. Sci.*, 2022, **600**, 154159.

85 J. Yang, J. Xian, Q. Liu, Y. Sun and G. Li, *J. Energy Chem.*, 2022, **69**, 524–530.

86 M. Winter and J. O. Besenhard, *Electrochim. Acta*, 1999, **45**, 31–50.

87 J. Eaves-Rathert, K. Moyer-Vanderburgh, K. Wolfe, M. Zohair and C. L. Pint, *Energy Storage Mater.*, 2022, **53**, 552–558.

88 L. D. Ellis, B. N. Wilkes, T. D. Hatchard and M. N. Obrovac, *J. Electrochem. Soc.*, 2014, **161**, A416.

89 X. Zhao, N. Liu, C. Mu, B. Qin and L. Wang, *J. Colloid Interface Sci.*, 2024, **669**, 647–656.

90 H. Yuan, F. Ma, X. Wei, J. Lan, Y. Liu, Y. Yu, X. Yang and H. S. Park, *Adv. Energy Mater.*, 2020, **10**, 2001418.

91 Q. Zhang, J. Mao, W. K. Pang, T. Zheng, V. Sencadas, Y. Chen, Y. Liu and Z. Guo, *Adv. Energy Mater.*, 2018, **8**, 1703288.

92 L. Chen, X. He, H. Chen, S. Huang and M. Wei, *J. Mater. Chem. A*, 2021, **9**, 22048–22055.

93 J. Y. Hwang, S. T. Myung and Y. K. Sun, *Adv. Funct. Mater.*, 2018, **28**, 1802938.

94 X. Sui, X. Huang, H. Pu, Y. Wang and J. Chen, *Nano Energy*, 2021, **83**, 105797.

95 Z. Tong, T. Kang, Y. Wu, F. Zhang, Y. Tang and C. Lee, *Nano Res.*, 2022, **15**, 7220–7226.

96 F. Liu, P. Zuo, J. Li, P. Shi, Y. Shao, L. Chen, Y. Tan and T. Ma, *J. Energy Chem.*, 2024, **93**, 282–288.

97 B. Cao, H. Liu, X. Zhang, P. Zhang, Q. Zhu, H. Du, L. Wang, R. Zhang and B. Xu, *Nano-Micro Lett.*, 2021, **13**, 202.

98 Z. Li, Z. Long, H. Dai, Z. Yan, Q. Wang, K. Wang, Q. Wei and H. Qiao, *Chem. Eng. J.*, 2024, **498**, 155814.

99 P. Li, H. Yang and Q. Wang, *J. Energy Storage*, 2024, **84**, 110823.

100 Y. Li, J. Zhang, Q. Chen, X. Xia and M. Chen, *Adv. Mater.*, 2021, **33**, 2100855.

101 Q. Zhang, M. Chen, J. Wang, C. Zhao, F. Cao, H. Li, H. Cong and C. Zhang, *J. Mater. Chem. A*, 2023, **11**, 5056–5066.

102 Y. Feng, M. Xu, T. He, B. Chen, F. Gu, L. Zu, R. Meng and J. Yang, *Adv. Mater.*, 2021, **33**, 2007262.

103 S. Zhang, F. Ling, L. Wang, R. Xu, M. Ma, X. Cheng, R. Bai, Y. Shao, H. Huang, D. Li, Y. Jiang, X. Rui, J. Bai, Y. Yao and Y. Yu, *Adv. Mater.*, 2022, **34**, 2201420.

104 H. Lv, X. Wang, Y. Yang, T. Liu and L. Zhang, *Acta Phys. -Chim. Sin.*, 2023, **39**, 2210014.

105 W. Liu, J. Yuan, Y. Hao, H. Maleki Kheimeh Sari, J. Wang, A. Kakimov, W. Xiao, J. Qin, W. Li, C. Xie, J. Hu, J. Peng and X. Li, *J. Mater. Chem. A*, 2020, **8**, 23395–23403.

106 Y. Fang, D. Luan, Y. Chen, S. Gao and X. W. Lou, *Angew. Chem., Int. Ed.*, 2020, **59**, 2644–2648.

107 J. Ni, S. Fu, C. Wu, J. Maier, Y. Yu and L. Li, *Adv. Mater.*, 2016, **28**, 2259–2265.

108 M. Fan, Z. Lin, P. Zhang, X. Ma, K. Wu, M. Liu and X. Xiong, *Adv. Energy Mater.*, 2021, **11**, 2003037.

109 T. Yao, H. Wang, Y. Qin, J. Shi and Y. Cheng, *Composites, Part B*, 2023, **253**, 110557.

110 L. Wang, Z. Han, Q. Zhao, X. Yao, Y. Zhu, X. Ma, S. Wu and C. Cao, *J. Mater. Chem. A*, 2020, **8**, 8612–8619.

111 H. Ye and Y. Li, *InfoMat*, 2022, **4**, e12291.

112 X. Gao, L. Wang, J. Cheng, J. Zhao and X. Liu, *Chin. Chem. Lett.*, 2025, **36**, 110247.

113 X. Zhou, Y. Wang, Y. Gu, J. Su, Y. Liu, Y. Yin, S. Yuan, J. Ma, Z. Jin and J.-L. Zuo, *Matter*, 2024, **7**, 3069–3082.

114 X. Ren, Q. Wang, Y. Pu, Q. Sun, W. Sun and L. Lu, *Adv. Mater.*, 2023, **35**, 2304120.

115 Á. Bonilla, G. A. Ortega-Moreno, M. C. Bernini, J. L. Gómez-Cámer, L. I. Barbosa and Á. Caballero, *J. Power Sources*, 2024, **608**, 234613.

116 C. Ye, Y. Jiao, D. Chao, T. Ling, J. Shan, B. Zhang, Q. Gu, K. Davey, H. Wang and S. Z. Qiao, *Adv. Mater.*, 2020, **32**, 1907557.

117 L. Zhou, H. Pan, G. Yin, Y. Xiang, P. Tan, X. Li, Y. Jiang, M. Xu and X. Zhang, *Adv. Funct. Mater.*, 2024, **34**, 2314246.

118 Q. Zeng, X. Li, W. Gong, S. Guo, Y. Ouyang, D. Li, Y. Xiao, C. Tan, L. Xie, H. Lu, Q. Zhang and S. Huang, *Adv. Energy Mater.*, 2022, **12**, 2104074.

119 Y. Liu, F. Wu, Z. Hu, F. Zhang, K. Wang, L. Li and R. Chen, *Angew. Chem., Int. Ed.*, 2024, **63**, e202402624.

120 X. Li, Z. Yan, J. Zhang, Z. Huang, F. Li, L. Yang, J. Huang, G. Wang and G. Xu, *Chem. Eng. J.*, 2024, **493**, 152554.

121 Z. Cheng, J. Lian, J. Zhang, S. Xiang, B. Chen and Z. Zhang, *Adv. Sci.*, 2024, **11**, 2404834.

122 S. Bai, X. Liu, K. Zhu, S. Wu and H. Zhou, *Nat. Energy*, 2016, **1**, 16094.

123 J. Bi, L. Chen, X. Yan, J. Guo, Y. Tang, M. Jian, S. Meng, K. Liao, J. Yu, W. Yao, T. He and H. Zhao, *Chem. Eng. J.*, 2024, **496**, 154347.

124 J. Wang, X. Zhang, X. Wang, J. Liu, S. Li, Y. Nie, K. Zong, X. Zhang, H. Meng, M. Jin, L. Yang, X. Wang and Z. Chen, *Adv. Energy Mater.*, 2024, **14**, 2402072.

125 Y. Fei, Z. Li, P. Li, X. Zhang, Z. Xu, W. Deng, H. Zhang and G. Li, *ACS Appl. Mater. Interfaces*, 2024, **16**, 53833–53842.

126 G. Han, T. Deng, X. Jiao, X. Men, J. Wang, Y. Wang and Q. Zhai, *Ionics*, 2021, **27**, 5115–5125.

127 T. Zhao, N. L. Bell, G. Chisholm, B. Kandasamy, D. L. Long and L. Cronin, *Energy Environ. Sci.*, 2023, **16**, 2603–2610.

128 W. Lu, Z. Pang, A. Lamaire, F. Liu, S. Dai, M. L. Pinto, R. Demir-Cakan, K. Ooi Tan, V. Van Speybroeck, V. Pimenta and C. Serre, *Small Sci.*, 2024, **4**, 2300339.

129 S. Li, J. Lin, Y. Ding, P. Xu, X. Guo, W. Xiong, D. Wu, Q. Dong, J. Chen and L. Zhang, *ACS Nano*, 2021, **15**, 13803–13813.

130 S. Guo, Y. Xiao, J. Wang, Y. Ouyang, X. Li, H. Deng, W. He, Q. Zeng, W. Zhang, Q. Zhang and S. Huang, *Nano Res.*, 2021, **14**, 4556–4562.

131 Y. Jiang, H. Liu, X. Tan, L. Guo, J. Zhang, S. Liu, Y. Guo, J. Zhang, H. Wang and W. Chu, *ACS Appl. Mater. Interfaces*, 2017, **9**, 25239–25249.

132 J. Balach, T. Jaumann, M. Klose, S. Ostwald, J. Eckert and L. Giebeler, *Adv. Funct. Mater.*, 2015, **25**, 5285–5291.

133 X. Fang, Y. Jiang, K. Zhang, G. Hu and W. Hu, *New J. Chem.*, 2021, **45**, 2361–2365.

134 X. Song, R. Huang, X. Zhang, Q. Chang, S. Kim, D. Jeong, Q. Hou, J. Kim, E. H. Ang, X. Su, X. Feng and H. Xiang, *Adv. Sci.*, 2024, **11**, 2407984.

135 L. Jianming, Z. Jin, J. Shang and Z. Jianguo, *RSC Adv.*, 2023, **13**, 12792–12798.

136 F. Jin, Y. Ning, B. Wang, Z. Ren, H. Luo, Z. Zhang, N. Zhang and D. Wang, *J. Power Sources*, 2023, **565**, 232917.

137 X. Ge, H. Di, P. Wang, X. Miao, P. Zhang, H. Wang, J. Ma and L. Yin, *ACS Nano*, 2020, **14**, 16022–16035.

138 X. Zhou, Z. Yu, Y. Yao, Y. Jiang, X. Rui, J. Liu and Y. Yu, *Adv. Mater.*, 2022, **34**, 2200479.

139 E. Zhang, X. Hu, L. Meng, M. Qiu, J. Chen, Y. Liu, G. Liu, Z. Zhuang, X. Zheng, L. Zheng, Y. Wang, W. Tang, Z. Lu, J. Zhang, Z. Wen, D. Wang and Y. Li, *J. Am. Chem. Soc.*, 2022, **144**, 18995–19007.

140 F. Xiao, X. Yang, H. Wang, J. Xu, Y. Liu, D. Y. W. Yu and A. L. Rogach, *Adv. Energy Mater.*, 2020, **10**, 2000931.

141 J. Feng, C. Shi, H. Dong, C. Zhang, W. Liu, Y. Liu, T. Wang, X. Zhao, S. Chen and J. Song, *J. Energy Chem.*, 2023, **86**, 135–145.

142 W. Song, X. Yang, T. Zhang, Z. Huang, H. Wang, J. Sun, Y. Xu, J. Ding and W. Hu, *Nat. Commun.*, 2024, **15**, 1005.

143 Y. Xie, J. Cao, X. Wang, W. Li, L. Deng, S. Ma, H. Zhang, C. Guan and W. Huang, *Nano Lett.*, 2021, **21**, 8579–8586.

144 Y. Yao, C. Zhou, Z. Zhao, G. Chang, J. Wei, K. Huang, J. Xie, J. Li and X. Yang, *Carbon*, 2024, **223**, 119018.

145 C. Senthil and H. Y. Jung, *Coord. Chem. Rev.*, 2024, **500**, 215493.

146 C. Hou, H. Wang, C. Li and Q. Xu, *Energy Environ. Sci.*, 2020, **13**, 1658–1693.

147 Y. Li, G. Chen, J. Mou, Y. Liu, S. Xue, T. Tan, W. Zhong, Q. Deng, T. Li, J. Hu, C. Yang, K. Huang and M. Liu, *Energy Storage Mater.*, 2020, **28**, 196–204.

148 X. Li, Y. Xiao, Q. Zeng, L. Xu, S. Guo, C. Zheng, Q. Zhang and S. Huang, *Nano Energy*, 2023, **116**, 108813.

149 S. Ji, Y. Qu, T. Wang, Y. Chen, G. Wang, X. Li, J. Dong, Q. Chen, W. Zhang, Z. Zhang, S. Liang, R. Yu, Y. Wang, D. Wang and Y. Li, *Angew. Chem., Int. Ed.*, 2020, **59**, 10651–10657.

150 R. Ryoo, J. Kim, C. Jo, S. W. Han, J. Kim, H. Park, J. Han, H. S. Shin and J. W. Shin, *Nature*, 2020, **585**, 221–224.

151 Y. Wang, H. Su, Y. He, L. Li, S. Zhu, H. Shen, P. Xie, X. Fu, G. Zhou, C. Feng, D. Zhao, F. Xiao, X. Zhu, Y. Zeng, M. Shao, S. Chen, G. Wu, J. Zeng and C. Wang, *Chem. Rev.*, 2020, **120**, 12217–12314.

152 F. Xiao, H. Wang, J. Xu, W. Yang, X. Yang, D. Y. W. Yu and A. L. Rogach, *Adv. Energy Mater.*, 2021, **11**, 2100989.

153 Z. Wu, L. Wang, S. Chen, X. Zhu, Q. Deng, J. Wang, Z. Zeng and S. Deng, *Chem. Eng. J.*, 2021, **404**, 126579.

154 B. Ding, Z. Fan, Q. Lin, J. Wang, Z. Chang, T. Li, J. Henzie, J. Kim, H. Dou, X. Zhang and Y. Yamauchi, *Small Methods*, 2019, **3**, 1900277.

155 R. Chu, T. T. Nguyen, Y. Bai, N. H. Kim and J. H. Lee, *Adv. Energy Mater.*, 2022, **12**, 2102805.

156 C. Zhao, G. Xu, Z. Yu, L. Zhang, I. Hwang, Y. Mo, Y. Ren, L. Cheng, C. Sun, Y. Ren, X. Zuo, J. Li, S. Sun, K. Amine and T. Zhao, *Nat. Nanotechnol.*, 2021, **16**, 166–173.

157 T. Zhao, H. Wu, X. Wen, J. Zhang, H. Tang, Y. Deng, S. Liao and X. Tian, *Coord. Chem. Rev.*, 2022, **468**, 214642.

158 X. Chen, J. Liu, H. Jiang, C. Zhan, Y. Gao, J. Li, H. Zhang, X. Cao, S. Dou and Y. Xiao, *Energy Storage Mater.*, 2024, **65**, 103168.

159 S. Mondal, P. Samanta, R. Sahoo, T. Kuila and M. C. Das, *Chem. Eng. J.*, 2023, **470**, 144340.

160 S. Deng, B. Xu, J. Zhao, C. W. Kan and X. Liu, *Angew. Chem., Int. Ed.*, 2024, **63**, e202401996.

161 J. Liu, Y. Zhou, G. Xing, M. Qi, Z. Tang, O. Terasaki and L. Chen, *Adv. Funct. Mater.*, 2024, **34**, 2312636.

162 C. Miao, X. Wang, D. Guan, J. Li, J. Li and J. Xu, *Angew. Chem., Int. Ed.*, 2024, **63**, e202410208.

163 D. Bi, T. Zhao, Q. Lai, J. Zhao, S. A. Grigoriev and Y. Liang, *J. Alloys Compd.*, 2024, **1002**, 175448.

164 Y. Wang, J. Song and W. Wong, *Angew. Chem., Int. Ed.*, 2023, **62**, e202218343.

165 P. Wu, Y. Cao, H. Cao, Y. Liu, X. Huang, J. Zhang, Y. Cao, Y. Long, Y. Zhai, Z. Wu, Q. Zheng and D. Lin, *Chem. Eng. J.*, 2023, **474**, 145955.

166 X. Hui, Z. Zhan, Z. Zhang, J. Yu, P. Jiang, Z. Dang, J. Wang, S. Cai, Y. Wang and Z. Xu, *ACS Nano*, 2024, **18**, 25237–25248.

167 Y. Lee, Y. Jeoun, J. H. Kim, J. Shim, K. Ahn, S. Yu and Y. Sung, *Adv. Funct. Mater.*, 2024, **34**, 2310884.

168 M. Chen, W. Fu, C. Hou, Y. Zhu and F. Meng, *Energy Storage Mater.*, 2025, **80**, 104380.

169 K. Sun, J. Pang, Y. Zheng, F. Xing, R. Jiang, J. Min, J. Ye, L. Wang, Y. Luo, T. Gu and L. Chen, *J. Alloys Compd.*, 2022, **923**, 166470.

170 X. Li, Q. Liu, X. Ma, P. Liu, D. Wang, X. Yu and Y. Liu, *J. Mater. Chem. A*, 2023, **11**, 19566–19577.

171 Y. Liu, C. Gao, Y. Sun, X. Hao, Z. Pi, M. Yang, X. Zhao and K. Cai, *Chem. Eng. J.*, 2024, **490**, 151535.

172 K. Chen, H. Guo, W. Li and Y. Wang, *ACS Appl. Mater. Interfaces*, 2021, **13**, 54990–54996.

173 M. Idrees, S. Batool, W. Hu and D. Chen, *Small*, 2024, **20**, 2402266.

174 Y. Zeng, Y. Wang, Q. Jin, Z. Pei, D. Luan, X. Zhang and X. W. Lou, *Angew. Chem., Int. Ed.*, 2021, **60**, 25793–25798.

175 K. Sun, Y. Shen, J. Min, J. Pang, Y. Zheng, T. Gu, G. Wang and L. Chen, *Chem. Eng. J.*, 2023, **454**, 140394.

176 G. Yuan, Y. Liu, J. Xia, Y. Su, W. Wei, Y. Zhu, Y. An, H. Wu, Q. Xu and H. Pang, *Nano Res.*, 2023, **16**, 6881–6889.